Ongoing, rational calibration of reward-driven perceptual biases

Yunshu Fan, Joshua I. Gold, and Long Ding

Department of Neuroscience
Neuroscience Graduate Group
University of Pennsylvania, Philadelphia, PA, USA

Corresponding author:

Long Ding
Department of Neuroscience
Perelman School of Medicine
University of Pennsylvania
D403 Richards Laboratories
3700 Hamilton Walk
Philadelphia, PA 19104
e-mail: lding@pennmedicine.upenn.edu
phone: 215-898-9656

Abstract

Decision-making is often interpreted in terms of normative computations that maximize a particular reward function for stable, average behaviors. Aberrations from the reward-maximizing solutions, either across subjects or across different sessions for the same subject, are often interpreted as reflecting poor learning or physical limitations. Here we show that such aberrations may instead reflect the involvement of additional satisficing and heuristic principles. For an asymmetric-reward perceptual decision-making task, three monkeys produced adaptive biases in response to changes in reward asymmetries and perceptual sensitivity. Their choices and response times were consistent with a normative accumulate-to-bound process. However, their context-dependent adjustments to this process deviated slightly but systematically from the reward-maximizing solutions. These adjustments were instead consistent with a rational process to find satisficing solutions based on the gradient of each monkey's reward-rate function. These results suggest new dimensions for assessing the rational and idiosyncratic aspects of flexible decision-making.

Introduction

Normative theory has played an important role in our understanding of how the brain forms decisions. For example, many perceptual, memory, and reward-based decisions show inherent trade-offs between speed and accuracy. These trade-offs are parsimoniously captured by a class of sequential-sampling models, such as the drift-diffusion model (DDM), that are based on the accumulation of noisy evidence over time to a pre-defined threshold value, or bound (Ratcliff, 1978; Gold and Shadlen, 2002; Bogacz et al., 2006; Krajbich et al., 2010). These models have close ties to statistical decision theory, particularly the sequential probability ratio test that can, under certain assumptions, maximize expected accuracy for a given number of samples or minimize the number of samples needed for a given level of accuracy (Barnard, 1946; Wald, 1947; Wald and Wolfowitz, 1948). However, even when these models provide good descriptions of the average behavior of groups of subjects, they may not capture the substantial variability in behavior that can occur across individuals and task conditions. The goal of this study was to better understand the principles that govern this variability, in particular how these principles relate to normative theory.

We focused on a perceptual decision-making task with asymmetric rewards. For this task, both human and animal subjects tend to make decisions that are biased towards the percept associated with the larger payoff (e.g. Maddox and Bohil, 1998; Voss et al., 2004; Diederich and Busemeyer, 2006; Liston and Stone, 2008; Serences, 2008; Feng et al., 2009; Simen et al., 2009; Nomoto et al., 2010; Summerfield and Koechlin, 2010; Teichert and Ferrera, 2010; Gao et al., 2011; Leite and Ratcliff, 2011; Mulder et al., 2012; Wang et al., 2013; White and Poldrack, 2014). These biases are roughly consistent with a rational strategy to maximize a particular reward function that depends on both the speed and accuracy of the decision process, such as the reward rate per trial or per unit time (Gold and Shadlen, 2002; Bogacz et al, 2006). This strategy can be accomplished via context-dependent adjustments in a DDM-like decision process along two primary dimensions (Fig. 1A): 1) the momentary sensory evidence, via the drift rate; and 2) the decision rule, via the relative bound heights that govern how much evidence is needed for each alternative. Subjects tend to make adjustments along one or both of these dimensions to produce overall biases that are consistent with normative theory, but with substantial individual variability (Voss et al., 2004; Cicmil et al., 2015; Bogacz et al., 2006; Simen et al., 2009; Summerfield and Koechlin, 2010; Leite and Ratcliff, 2011; Mulder et al., 2012; Goldfarb et al., 2014).

To better understand the principles that govern these kinds of idiosyncratic behavioral patterns, we trained three monkeys to perform a response-time (RT), asymmetric-reward decision task with mixed perceptual uncertainty (Fig. 1B). Like human subjects, the monkeys showed robust decision biases toward the large-reward option. These biases were sensitive to not just the reward asymmetry, as has been shown previously, but also to experience-dependent changes in perceptual sensitivity. These biases were consistent with adjustments to both the momentary evidence and decision rule in the

DDM. However, these two adjustments favored the large- and small-reward choice, respectively, leading to nearly, but not exactly, maximal reward rates. We accounted for these adjustments in terms of a satisficing, gradient-based learning model that calibrated biases to balance the relative influence of perceptual and reward-based information on the decision process. Together, the results imply the broad applicability of normative theory, including sequential-sampling and heuristic-based strategies to understand how the brain combines uncertain sensory input and internal preferences to form decisions that can vary considerably across individuals and task conditions.

Results

We trained three monkeys to perform the asymmetric-reward random-dot motion discrimination ("dots") task (Fig. 1B). All three monkeys were initially trained on a symmetric-reward version of the task for which they were required to make fast eye movements (saccades) in the direction congruent with the global motion of a random-dot kinematogram to receive juice reward. They then performed the asymmetric-reward versions that were the focus of this study. Specifically, in blocks of 30–50 trials, we alternated direction-reward associations between a "LR-Right" reward context (the large reward was paired with a correct rightward saccade and the small reward was paired with a correct leftward saccade) and the opposite "LR-Left" reward context. We also varied the ratio of large versus small reward magnitudes ("reward ratio") across sessions for each monkey. Within a block, we randomly interleaved motion stimuli with different directions and motion strengths (expressed as coherence, the fraction of dots moving in the same direction). We monitored the monkey's choice (which saccade to make) and RT (when to make the saccade) on each trial.

The monkeys' biases reflected changes in reward context and perceptual sensitivity

For the asymmetric-reward task, all three monkeys tended to make more choices towards the large-reward option, particularly when the sensory evidence was weak. These choice biases corresponded to horizontal shifts in the psychometric function describing the probability of making a rightward choice as a function of signed motion coherence (negative for leftward motion, positive for rightward motion; Fig. 2A). However, these biases differed in detail for the three monkeys. For example, bias magnitude tended to be smallest in monkey F. Moreover, bias magnitude tended to decrease with session number for all three monkeys, although this tendency was statistically significant only for monkey C after accounting for co-variations with reward rate (Fig. 2B, middle). Additionally, each monkey showed steady increases in perceptual sensitivity (steepness of the psychometric function), which initially dropped relative to values from the symmetric-reward task then tended to increase with more experience with asymmetric rewards (Fig. 2B, top; H_0: partial Spearman's ρ of sensitivity versus session index after accounting for session-specific reward ratios = 0, $p<0.01$ in all cases, except LR-Left for monkey C, for which $p=0.57$). These improvements did not involve systematic changes in lapse rates, which remained near zero across sessions (Fig. 2B, bottom), implying

that the monkeys knew how to perform the task. However, these increases in sensitivity did correspond to systematic decreases in choice biases in some, but not all, cases (3 monkeys x 2 reward contexts; Fig. 2C), which is expected for an optimal process that maximizes reward per trial (RTrial; Fig. S2). Compared to these optimal biases, the monkey's biases tended to vary over sessions and overshoot for monkeys F and C (Fig. 2D).

To better understand the computational principles that governed these idiosyncratic biases, while also taking into account systematic relationships between the choice and RT data, we fit single-trial RT data (i.e., we modeled full RT distributions, not just mean RTs) from individual sessions to a DDM. We used a hierarchical-DDM (HDDM) method that assumes that parameters from individual sessions are samples from a group distribution (Wiecki et al., 2013). The HDDM had six parameters for each reward context. Four were from a basic DDM (Fig. 1A): *a,* the total bound height, representing the distance between the two choice bounds; *k*, a scaling factor that converts sensory evidence (motion strength and direction) to the drift rate; and t_0 and t_1, non-decision times for leftward and rightward choices, respectively. The additional two parameters provided biases that differed in terms of their effects on the full RT distributions (Supplementary Fig. 2): *me*, which is additional momentary evidence that is added to the motion evidence at each accumulating step and has asymmetric effects on the two choices and on correct versus error trials (positive values favor the rightward choice); and *z*, which determines the decision rules for the two choices and tends to have asymmetric effects on the two choices but not on correct versus error trials (values >0.5 favor the rightward choice). A DDM variant with collapsing bounds provided qualitatively similar results as the HDDM. Thus, subsequent analyses use the model with fixed bounds, unless otherwise noted. Example fits for this model are shown in Fig. 3, and summaries of best-fitting parameters and goodness-of-fit metrics are provided in Supplementary Table 1.

The DDM fits provided a parsimonious account of both the choice and RT data. Consistent with the results from the logistic analyses, the HDDM analyses showed that the monkeys made systematic improvements in psychometric sensitivity (H_0: partial Spearman's ρ of sensitivity versus session index after accounting for session-specific reward ratios=0, $p<0.01$ in all cases except $p=0.06$ for LR-Left for monkey A). Moreover, there was a negative correlation between psychometric sensitivity and choice bias (H_0: partial Spearman's ρ of sensitivity versus total bias after accounting for session-specific reward ratios=0, $p<0.001$ in all cases). These fits ascribed the choice biases to changes in both the momentary evidence (*me*) and the decision rule (*z*) of the decision process, as opposed to either parameter alone (Supplementary Table 2). These fits also indicated context-dependent differences in non-decision times, which were smaller for all large-reward choices for all three monkeys except in LR-Right context for monkey C and A (*t*-test, $p<0.05$).

The monkeys' bias adjustments were adaptive with respect to optimal reward-rate functions

To try to identify common principles that governed these monkey- and context-dependent decision biases, we analyzed behavior with respect to optimal benchmarks based on certain reward-rate functions. We focused on reward per unit time (RR) and per trial (RTrial), which for this task are optimized in a DDM framework by adjusting momentary-evidence (*me*) and decision-rule (*z*) biases, such that both favor the large-reward choice. However, the magnitudes of these optimal adjustments depend on other task parameters (a, k, t_0, and t_1, non-bias parameters from the DDM, plus the ratio of the two reward sizes and inter-trial intervals; Supplementary Fig. 12) that can vary from session to session. Thus, to determine the optimal adjustments, we performed DDM simulations with the fitted HDDM parameters from each session, using different combinations of *me* and *z* values (Fig. 4A). As reported previously (Bogacz et al., 2006; Simen et al., 2009), when the large reward was paired with the leftward choice, the optimal strategy used $z<0.5$ and $me<0$ (Fig. 4B, top panels, purple and orange circles for RR and RTrial, respectively). Conversely, when the larger reward was paired with the rightward choice, the optimal strategy used $z>0.5$ and $me>0$ (Fig. 4B, bottom panels).

The monkeys' adjustments of momentary-evidence (*me*) and decision-rule (*z*) biases showed both differences and similarities with respect to these optimal predictions (Fig. 4B, black circles; similar results were obtained using fits from a model with collapsing bounds, Supplementary Fig. 5). In the next section, we consider the differences, in particular the apparent use of shifts in *me* in the adaptive direction (i.e., favoring the large-reward choice) but of a magnitude that was larger than predicted, along with shifts in *z* that tended to be in the non-adaptive direction (i.e., favoring the small-reward choice). Here we focus on the similarities and show that the monkeys' decision biases were adaptive with respect to the reward-rate function in four ways (RTrial provided slightly better predictions of the data and thus are presented in the main figures; results based on RR are presented in the Supplementary Figures).

First, the best-fitting *me* and *z* values from each monkey corresponded to near-maximal reward rates (Fig. 5A). We compared the optimal values of reward per trial (RTrial_{max}) to the values predicted from the monkeys' best-fitting *me* and *z* adjustments ($\text{RTrial}_{predict}$). Both $\text{RTrial}_{predict}$ and RTrial_{max} depended on the same non-bias parameters in the HDDM fits that were determined per session (a, k, t_0, and t_1) and thus are directly comparable. Their ratios tended to be nearly, but slightly less than, one (mean ratio: 0.977, 0.984, and 0.982 for monkeys F, C, and A, respectively) and remained relatively constant across sessions (H_0: slopes of linear regressions of these ratios versus session number=0, $p>0.05$ for all three monkeys). Similar results were also obtained using the monkeys' realized rewards, which closely matched $\text{RTrial}_{predict}$ (Spearman's $\rho=0.991$, 0.979, and 0.906 for monkeys F, C, and A, respectively, $p<0.0001$ in all three cases). These results reflected the shallow plateau in the RTrial function near its peak (Fig. 5B), such that the monkeys' actual adjustments of *me* and *z* were within the contours for 97% RTrial_{max} in most sessions (Fig. 5C; see Supplementary Fig. 6 for results using RR). Thus, the monkeys' overall choice biases were consistent with strategies that lead to nearly optimal reward outcomes.

Second, the across-session variability of each monkey's decision biases was predicted by idiosyncratic features of the reward functions. The reward functions were, on average, different for the two reward contexts and each of the three monkeys (Fig. 6A). These differences included the size of the near-maximal plateau (red patch), which determined the level of tolerance in RTrial for deviations from optimal adjustments in *me* and *z*. This tolerance corresponded to the session-by-session variability in each monkey's *me* and *z* adjustments (Fig. 6B). In general, monkey F had the smallest plateaus and tended to use the narrowest range of *me* and *z* adjustments across sessions. In contrast, monkey A had the largest plateaus and tended to use the widest range of *me* and *z* adjustments (Pearson's ρ between the size of the 97% RTrial contour, in pixels, and the sum of the across-session variances in each monkeys' *me* and *z* adjustments=0.83, p=0.041). Similar analyses using the RR function produced qualitatively similar results (Supplementary Fig. 8B).

Third, the session-by-session adjustments in both *me* and *z* corresponded to particular features of each monkey's context-specific reward function. The shape of this function, including the orientation of the plateau with respect to *z* and *me*, depended on the monkey's perceptual sensitivity and the reward ratio for the given session. The monkeys' *me* and *z* adjustments varied systematically with this orientation (Fig. 6C and D for RTrial, Supplemental Fig. 8C and D for RR). This result was not an artifact of the fitting procedure, which was able to recover appropriate, simulated bias parameter values regardless of the values of non-bias parameters that determine the shape of the reward function (Supplementary Fig. 9).

Fourth, the monkeys' *me* and *z* adjustments were correlated with the values that would maximize RTrial, given the value of the other parameter for the given session and reward context (Fig. 6E for RTrial, Supplemental Fig. 8E for RR). These correlations were substantially weakened by shuffling the session-by-session reward functions (Supplementary Fig. 7). Together, these results suggest that all three monkeys used biases that were adaptively calibrated with respect to the reward information and perceptual sensitivity of each session.

The monkeys' adaptive adjustments were consistent with a satisficing, gradient-based learning process

Thus far, we showed that all three monkeys adjusted their decision strategies in a manner that matched many features of the optimal predictions based on their idiosyncratic, context-specific reward-rate functions. However, their biases did not match the optimal predictions exactly. Specifically, all three monkeys used shifts in *me* favoring the large-reward choice (adaptive direction) but of a magnitude that was larger than predicted, along with shifts in *z* favoring the small-reward choice (non-adaptive direction). We next consider if and how a consistent, adaptive process used by all three monkeys could lead to these idiosyncratic and not-quite optimal patterns of adjustments.

We propose that a gradient-based satisficing model can account for these patterns of

adjustments. The intuition for the model is shown in Fig. 7. The lines on the RTrial heatmap represent the trajectories of a gradient-tracking procedure that adjusts *me* and *z* values to increase RTrial until reaching 97% of the maximum possible value. Gradient lines are color-coded based on how *me* and *z* values at the end points relate to the optimal *me* and *z* values. For example, consider adjusting *me* and *z* by following all of the magenta gradient lines until their endpoints. This procedure would result in *me* shifts in the adaptive direction with magnitudes larger than the optimal *me*, plus *z* shifts in the non-adaptive direction. In other words, as long as the initial *me* and *z* values fall within the area covered by the magenta lines, the positive gradient-tracking procedure would lead to a good-enough solution with over-shifted *me* and non-adaptive *z* values similar to what we found in the monkeys' data.

We simulated this process with the reward function derived for each reward context, session, and monkey, using different starting points and a termination rule corresponding to achieving the estimated $RTrial_{predict}$ from those conditions (see above). This process is illustrated for LR-Left blocks in an example session from monkey C (Fig. 8A). We estimated the unbiased *me* and *z* values as the midpoints between their values for LR-Left and LR-Right blocks (square). At this point, the RTrial gradient is larger along the *me* dimension than the *z* dimension, reflecting the tilt of the reward function. We set the initial point at baseline *z* and a very negative value of *me* (-90% of the highest coherence used in the session; overshoot in the adaptive direction) and referred to this setting as the "over-*me*" model. The *me* and *z* values were then updated in a step-wise fashion (magenta trace), according to the RTrial gradient, until the monkey's $RTrial_{predict}$ or better was achieved (magenta circle). The endpoint of this updating process was very close to monkey C's actual adjustment (gray circle). For comparison, three alternative models are illustrated. The "over-*z*" model selects *z* as the initial dimension and assumes updating from the baseline *me* and over-adjusted *z* values (blue, initial *z* set as 0.1 for the LR-Left context and 0.9 for the LR-Right context). The "over-both" model assumes updating from the over-adjusted *me* and *z* values (green). The "neutral" model assumes the same updating process but from the baseline *me* and baseline *z* (black). The endpoints from these alternative models deviated considerably from the monkey's actual adjustment.

The "over-*me*" model produced better predictions than the other three alternative models for all three monkeys. Of the four models, only the "over-*me*" model captured the monkeys' tendency to bias *me* toward the large-reward choice (positive Δme) and bias *z* toward the small-reward choice (negative Δz; Fig. 8B). In contrast, the "over-*z*" model predicted small adjustments in *me* and large adjustments in *z* favoring the large-reward choice; the "over-both" model predicted relatively large, symmetric *me* and z adjustments favoring the large-reward choice; and the "neutral" model predicted relatively small, symmetric adjustments in both *me* and *z* favoring the large-reward choice. Accordingly, for each monkey, the predicted and actual values of both Δme and Δz were most strongly positively correlated for predictions from the "over-*me*" model compared to the other models (Fig. 8C). The "over-*me*" model was also the only one of

the models we tested that recapitulated the measured relationships between both *me*- and *z*-dependent biases and session-by-session changes in the orientation of the RTrial function (Fig. 8D). Qualitatively similar results were obtained with a different criterion that stopped updating when RTrial reached a fixed 98% of $RTrial_{max}$, suggesting that the ability of the "over-*me*" model to mimic monkeys' performance did not simply result from setting session-specific final RTrial values.

Discussion

We analyzed the behavior of three monkeys performing a decision task that encouraged the use of both uncertain visual motion evidence and the reward context. All three monkeys made choices that were sensitive to the strength of the sensory evidence and were biased toward the larger-reward choice, which is roughly consistent with previous studies of humans and monkeys performing similar tasks (Maddox and Bohil, 1998; Voss et al., 2004; Diederich and Busemeyer, 2006; Liston and Stone, 2008; Serences, 2008; Feng et al., 2009; Simen et al., 2009; Nomoto et al., 2010; Summerfield and Koechlin, 2010; Teichert and Ferrera, 2010; Gao et al., 2011; Leite and Ratcliff, 2011; Mulder et al., 2012; Wang et al., 2013; White and Poldrack, 2014).However, we also found that these adjustments differed considerably in detail for the three monkeys, in terms of overall magnitude, dependence on perceptual sensitivity and offered rewards, and relationship to RTs. We quantified these effects with a logistic analysis and a commonly used model of decision-making, the drift-diffusion model (DDM), which allowed us to compare the underlying decision-related computations to hypothetical benchmarks that would maximize reward. We found that all three monkeys made reward context-dependent adjustments with two basic components: 1) an over-adjustment of the momentary evidence provided by the sensory stimulus (*me*) in favor of the large-reward option; and 2) an adjustment to the decision rule that governs the total evidence needed for each choice (*z*), but in the opposite direction (i.e., towards the small-reward option). These adjustments tended to provide nearly, but not exactly, maximal reward intake. We proposed a common heuristic strategy based on the monkeys' individual reward functions to account for the idiosyncratic adjustments across monkeys and across sessions within the same monkey.

Considerations for assessing optimality and rationality

Assessing decision optimality requires a model of the underlying computations. In this study, we chose the DDM for several reasons. First, it provided a parsimonious account of both the choice and RT data (Palmer et al., 2005; Ratcliff et al., 1999). Second, as discussed in more detail below, the DDM and related accumulate-to-bound models have provided useful guidance for identifying neural substrates of the decision process (Roitman and Shadlen, 2002; Ding and Gold, 2010; Ding and Gold, 2012; Hanks et al., 2011; Ratcliff et al., 2003; Rorie et al., 2010; Mulder et al., 2012; Summerfield and Koechlin, 2010; Frank et al., 2015). Third, these models are closely linked to normative theory, including under certain assumptions matching the statistical procedure known as the sequential probability ratio test that can optimally balance the speed and accuracy of

uncertain decisions (Barnard, 1946; Wald, 1947; Wald and Wolfowitz, 1948). These normative links were central to our ability to use the DDM to relate the monkeys' behavior to different forms of reward optimization.

Assessing optimality also requires an appropriate definition of the optimization goal. In our study, we mainly focused on the goal of maximizing reward rate (per trial or per unit of time). Based on this definition, the monkeys showed suboptimal reward-context-dependent adjustments. It is possible that the monkeys' were optimizing for a different goal, such as accuracy or a competition between reward and accuracy ("COBRA," Maddox and Bohil, 1998). However, the monkeys' behavior was not consistent with optimizing for these goals, either. Specifically, none of these goals would predict optimal *z* adjustment that favors the small reward choice: accuracy maximization would require unbiased decisions: *me*=0 and *z*=0.5, whereas COBRA would require *z* values with smaller magnitude (between 0.5 and those predicted for reward maximization alone), but still in the adaptive direction. Therefore, the monkeys' strategies were not consistent with simply maximizing commonly considered reward functions.

Deviations from optimal behavior are often ascribed to a lack of effort or poor learning. However, these explanations seem unlikely to be primary sources of suboptimality in our study. For example, lapse rates, representing the overall ability to attend to and perform the task, were consistently near zero for all three monkeys. Moreover, the monkeys' reward outcomes (RTrial or RR with respect to optimal values) did not change systematically with experience but instead stayed close to the optimal values. These results imply that the monkeys understood the task demands and performed consistently well over the course of our study. More importantly, the monkeys' reward-context-dependent adjustments were adapted to changes in the reward function due to session-specific reward ratios and motion coherences and the monkeys' daily variations of perceptual sensitivity and speed-accuracy trade-offs (Fig. 6E, Fig. S8). Based on these observations, we reasoned that the seemingly sub-optimal behaviors may instead reflect a common, adaptive, rational strategy that aimed to attain good-enough outcomes.

The gradient-based, satisficing model we proposed was based on these considerations to account for our results. We do not yet know how well this model generalizes to other tasks and conditions, but it exemplifies an additional set of general principles for assessing the rationality of decision-making behavior: an alternative satisficing (good-enough) goal, potential heuristic strategies based on the properties of the utility function, and flexible adaptation to changes in the external and internal conditions. Below we discuss the assumptions of our proposed model in more detail.

Adjustments with respect to the gradient of the utility function

In general, finding rational solutions through trial-and-error or stepwise updates requires a sufficient gradient in the utility function to drive learning (Sutton and Barto, 1998). Our proposed scheme couples a standard gradient-following algorithm with principles that have been used to explain and facilitate decisions with high uncertainties, time

pressures, and/or complexity to achieve a satisficing solution (Simon, 1966; Wierzbicki, 1982; Gigerenzer and Goldstein, 1996; Nosofsky and Palmeri, 1997; Goodrich et al., 1998; Sakawa and Yauchi, 2001; Goldstein and Gigerenzer, 2002; Stirling, 2003; Gigerenzer, 2010; Oh et al., 2016). This scheme complements but differs from a previously proposed satisficing strategy to account for human subjects' suboptimal calibration of the speed-accuracy trade-off via adjustments of the decision bounds of a DDM that favor robust solutions given uncertainties about the inter-trial interval (Zacksenhouse et al., 2010), In contrast, our proposed strategy focuses on reward-biased behaviors for a given speed-accuracy tradeoff and operates on reward per trial, which is, by definition, independent of inter-trial-interval. Our scheme was based on three key assumptions, as follows.

Our first key assumption was that the starting point for gradient following was not the unbiased state (i.e., me=0 and z=0.5) but an over-biased state. Notably, in many cases the monkeys could have performed as well or better than they did, in terms of optimizing reward rate, by making unbiased decisions. The fact that none did so prompted our assumption that their session-by-session adjustments tended to reduce, not inflate, biases. Specifically, we assumed that the initial experience of the asymmetric reward prompted an over-reaction to bias choices towards the large-reward alternative. In general, such an initial over-reaction is not uncommon, as other studies have shown excessive, initial biases that are reduced or eliminated with training (Gold et al., 2008; Jones, et al., 2015; Nikolaev et al., 2016). The over-reaction is also rational because the penalty is larger for an under reaction than for an overreaction. For example, in the average RTrial heatmaps for our task (Fig. 6A), the gradient dropped faster in the under-biased side than in the over-biased side. This pattern is generally true for tasks with sigmoid-like psychometric functions (for example, the curves in Supplementary Fig. 2). Our model further suggests that the nature of this initial reaction, which may be driven by individually tuned features of the reward function that can remain largely consistent even for equal-reward tasks (Supplementary Fig. 12) and then constrain the end-points of a gradient-based adjustment process (Fig. 8), may help account for the extensive individual variability in biases that has been reported for reward-biased perceptual tasks (Voss et al., 2004; Summerfield and Koechlin, 2010; Leite and Ratcliff, 2011; Cicmil et al., 2015)).

Our second key assumption was that from this initial, over-biased state, the monkeys made adjustments to both the momentary evidence (me) and decision rule (z) that generally followed the gradient of the reward function. The proposed step-wise adjustments occurred too quickly to be evident in behavior; e.g., the estimated biases were similar for the early and late halves in a block (data not shown). Instead, our primary support for this scheme was that the steady-state biases measured in each session were tightly coupled to the shape of the reward function for that session. It would be interesting to design tasks that might allow for more direct measurements of the updating process itself, for example, by manipulating both the initial biases and relevant reward gradient that might promote a longer adjustment process.

Our third key assumption was that the shallowness of the utility of the function around the peak supported satisficing solutions. Specifically, gradient-based adjustments, particularly those that use rapid updates based on implicit knowledge of the utility function, may only be sensitive to relatively large gradients. For our task, the gradients were much smaller around the peak, implying that there were large ranges of parameter values that provided such similar outcomes that further adjustments were not used. In principle, it is possible to change the task conditions to test if and how subjects might optimize with respect to steeper functions around the peak. For example, for RTrial, the most effective way to increase the gradient magnitude near the peak (i.e., reducing the area of the dark red patch) is to increase sensory sensitivity (*k*) and cautiousness (Supplementary Fig. 12; *a*; i.e., emphasizing accuracy over speed). For RR, the gradient can also be increased by increasing the time-out penalty (not shown). Despite some practical concerns about these manipulations (e.g., increasing time-out penalties can decrease motivation), it would be interesting to study their effects on performance in more detail. Such studies would help inform how constraints of the utility function govern decision strategies, including when to use satisficing or "good enough" instead of optimal ones like in this study (Simon, 1956; Simon, 1982).

Possible neural mechanisms

Our study benefitted greatly from the ability of each of the three monkeys to perform this complex decision task nearly optimally and with few lapses of attention over many sessions. It also benefitted from an RT task design that provided a richer set of constraints for inferring characteristics of the underlying decision process than choice data alone (Feng et al., 2009; Nomoto et al., 2010; Teichert and Ferrera, 2010). Together, these benefits establish a strong foundation for planned, future studies of the underlying neural mechanisms, which are informed by our present results.

Specifically, the DDM framework has been used effectively to identify and interpret neural substrates of key computational components of the decision process for symmetric-reward versions of the motion-discrimination task. For example, the momentary evidence is represented, in part, by motion-sensitive neurons in the middle temporal (MT) area of extrastriate visual cortex (Newsome et al., 1989). When the decision is indicated with an eye movement, the accumulation of momentary evidence into the decision variable is represented in several brain areas involved in preparing and executing the eye-movement response, including parts of the parietal and prefrontal cortex, the basal ganglia, and the superior colliculus (e.g. Shadlen and Newsome, 2001; Ding and Gold, 2012; Ding and Gold, 2010; Horwitz and Newsome, 2001). In broad strokes, the *me* adjustment that we found may be implemented as reward modulation of MT output and/or synaptic weights for the connections between different MT subpopulations and decision areas (Cicmil, et al., 2015). In contrast, the *z* adjustment may be implemented as reward context-dependent baseline changes in neural representations of the decision variable and/or the rule that determines the final choice (Lo and Wang, 2006; Rao, 2010; Lo et al., 2015; Wei et al., 2015). Finally, modulation of

non-decision times may be implemented as reward modulation in higher-order motor-planning regions and/or lower-level motor generation circuits.

To summarize, our results suggest that the monkeys' idiosyncratic decision-making adjustments under changing contexts may reflect a rational heuristic strategy operating on the gradient of their individual reward functions. This new view extends the more conventional reward maximization-based test of rationality and may help to account for individual variations in decision-making strategies. It also opens up new questions about how the brain acquires, retains, and uses the knowledge needed to make such flexible adjustments. Answers to these questions will add to our growing understanding of increasingly complex forms of decision-making.

Methods

Subjects

We used three rhesus macaques (*Macaca mulatta*), two male and one female, to study behavior on an asymmetric-reward reaction-time random-dot motion discrimination task (Fig. 1B, see below). Prior to this study, monkeys F and C had been trained extensively on the equal-reward RT version of the task (Ding and Gold, 2010, 2012b, a). Monkey A had been trained extensively on non-RT dots tasks (Connolly et al., 2009; Bennur and Gold, 2011), followed by >130 sessions of training on the equal-reward RT dots task. All training and experimental procedures were in accordance with the National Institutes of Health Guide for the Care and Use of Laboratory Animals and were approved by the University of Pennsylvania Institutional Animal Care and Use Committee.

Behavioral task

Our task (Fig. 1B) was based on the widely used random-dot motion discrimination task that typically has symmetric rewards (Roitman and Shadlen, 2002; Ding and Gold, 2010). Briefly, a trial started with presentation of a fixation point at the center of a computer screen in front of a monkey. Two choice targets appeared 0.5 s after the monkey acquired fixation. After a delay, the fixation point was dimmed and a random-dot kinematogram (speed: 6 °/s) was shown in a 5° aperture centered on the fixation point. For monkeys F and C, the delay duration was drawn from a truncated exponential distribution with mean=0.7 s, max=2.5 s, min=0.4 s. For monkey A, the delay was set as 0.75 s. The monkey was required to report the perceived global motion direction by making a saccade to the corresponding choice target at a self-determined time (a 50-ms minimum latency was imposed to discourage fast guesses). The stimulus was immediately turned off when the monkeys' gaze left the fixation window (4, 4, and 3° square windows for monkey F, C, and A, respectively). Correct choices (i.e., saccades to the target congruent with actual motion direction) were rewarded with juice. Error choices were not rewarded and instead penalized with a timeout before the next trial began (timeout duration: 3 s, 0.5-2 s, and 2.5 s, for monkeys F, C, and A, respectively).

On each trial, the motion direction was randomly selected toward one of the choice targets along the horizontal axis. The motion strength of the kinematogram was controlled as the fraction of dots moving coherently to one direction (coherence). On each trial, coherence was randomly selected from 0.032, 0.064, 0.128, 0.256, and 0.512 for monkeys F and C, and from 0.128, 0.256, 0.512, and 0.75 for monkey A. In a subset of sessions, coherence levels of 0.064, 0.09, 0.35, and/or 0.6 were also used for monkey A.

We imposed two types of reward context on the basic task. For the “LR-Left” reward context, correct leftward saccades were rewarded with a larger amount of juice than correct rightward saccades. For the “LR-Right” reward context, correct leftward saccades were rewarded with a smaller amount of juice than correct rightward saccades. The large:small reward ratio was on average 1.34, 1.91, and 2.45 for monkeys F, C, and A, respectively. Reward context was alternated between blocks and constant within a block. Block changes were signaled to the monkey with an inter-block interval of 5 s. The reward context for the current block was signaled to the monkey in two ways: 1) in the first trial after a block change, the two choice targets were presented in blue and green colors, for small and large rewards, respectively (this trial was not included for analysis); and 2) only the highest coherence level (near 100% accuracy) was used for the first two trials after a block change to ensure that the monkey physically experienced the difference in reward outcome for the two choices. For the rest of the block, choice targets were presented in the same color and motion directions and coherence levels were randomly interleaved.

Basic characterization of behavioral performance

Eye position was monitored using a video-based system (ASL) sampled at 240 Hz. RT was measured as the time from stimulus onset to saccade onset, the latter identified offline with respect to velocity (> 40°/s) and acceleration (> 8000°/s^2). Performance was quantified with psychometric and chronometric functions (Figs. 2 and 3), which describe the relationship of motion strength (signed coherence, *Coh*, which was the proportion of the dots moving in the same direction, positive for rightward motion, negative for leftward motion) with choice and RT, respectively. Psychometric functions were fitted to a logistic function (Equation (1)), in which $\boldsymbol{\lambda}$ is the error rate, or lapse rate, independent of the motion information; $\boldsymbol{\alpha}_0$ and ($\boldsymbol{\alpha}_0 + \boldsymbol{\alpha}_{\text{rew}}$) are the bias terms, which measures the coherence at which the performance was at chance level in the LR-Right and LR-Left reward contexts, respectively. $\boldsymbol{\beta}_0$ and ($\boldsymbol{\beta}_0 + \boldsymbol{\beta}_{\text{rew}}$) are the perceptual sensitivities in the LR-Right and LR-Left reward contexts, respectively.

$$P_{rightward\ choice} = \lambda + (1 - 2\,\lambda) \times \frac{1}{e^{-Sensitivity(Coh-Bias)}} \quad (1)$$

Reward-biased drift-diffusion model

To infer the computational strategies employed by the monkeys, we adopted the widely used accumulation-to-bound framework, the drift-diffusion model (DDM; Fig. 1A). In the

standard DDM, motion evidence is modeled as a random variable following a Gaussian distribution with a mean linearly proportional to the signed coherence and a fixed variance. The decision variable (DV) is modeled as temporal accumulation (integral) of the evidence, drifting between two decision bounds. Once the DV crosses a bound, evidence accumulation is terminated, the identity of the decision is determined by which bound is crossed, and the decision time is determined by the accumulation time. RT is modeled as the sum of decision time and saccade-specific non-decision times, the latter accounting for the contributions of evidence-independent sensory and motor processes.

To model the observed influences of motion stimulus and reward context on monkeys' choice and RT behavior, we introduced two reward context-dependent terms: *z* specifies the relative bound heights for the two choices and *me* specifies the equivalent momentary evidence that is added to the motion evidence at each accumulating step. Thus, for each reward context, six parameters were used to specify the decision performance: *a:* total bound height; *k*: proportional scaling factor converting evidence to the drift rate; t_0 and t_1: non-decision times for leftward and rightward choices, respectively; and *z* and *me.* Similar approaches have been used in studies of human and animal decision making under unequal payoff structure and/or prior probabilities (Voss et al., 2004; Bogacz et al., 2006; Diederich and Busemeyer, 2006; Summerfield and Koechlin, 2010; Hanks et al., 2011; Mulder et al., 2012).

To fit the monkeys' data, we implemented hierarchical DDM fitting using an open-source package in Python, which performs Bayesian estimates of DDM parameters based on single-trial RTs (Wiecki et al., 2013). This method assumes that parameters from individual sessions are samples from a group distribution. The initial prior distribution of a given parameter is determined from previous reports of human perceptual performance and is generally consistent with monkey performance on equal reward motion discrimination tasks (Ding and Gold, 2010; Matzke and Wagenmakers, 2009). The posterior distributions of the session- and group-level parameters are estimated with Markov chain Monte Carlo sampling.

For each dataset, we performed 5 chains of sampling with a minimum of 10000 total samples (range: 10000-20000; burn-in: 5000 samples) and inspected the trace, autocorrelation and marginal posterior histogram of the group-level parameters to detect signs of poor convergence. To ensure similar level of convergence across models, we computed the Gelman-Rubin statistic (R-hat) and only accepted fits with R-hat<1.01.

To assess whether reward context modulation of both *z* and *me* was necessary to account for monkeys' behavioral data, we compared fitting performance between the model with both terms ("full") and reduced models with only one term ("z-only" and "me-only"). Model selection was based on the deviance information criterion (DIC), with a smaller DIC value indicating a preferred model. Because DIC tends to favor more complex models, we bootstrapped the expected ΔDIC values, assuming the reduced models were the ground truth, using trial-matched simulations. For each session, we generated simulated data using the DDM, with single-session parameters fitted by *me*-

only or *z*-only HDDM models and with the number of trials for each direction × coherence × reward context combination matched to the monkey's data for that session. These simulated data were then re-fitted by all three models to estimate the predicted ΔDIC, assuming the reduced model as the generative model.

To test an alternative model, we also fitted monkeys' data to a DDM with collapsing bounds (Zylberberg et al., 2016). This DDM was constructed as the expected first-stopping-time distribution given a set of parameters, using the PyMC module (version 2.3.6) in Python (version 3.5.2). The three model variants, "full", "*me*-only" and "*z*-only", and their associated parameters were the same as in HDDM, except that the total bound distance decreases with time. The distance between the two choice bounds is set as $a/(1+e^{\beta(t-d)})$, where a is the initial bound distance, β determines the rate of collapsing, and d determines the onset of the collapse. Fitting was performed by computing the maximum *a posteriori* estimates, followed by Markov chain Monte Carlo sampling, of DDM parameters given the experimental RT data.

Optimality analysis

To examine the level of optimality of the monkeys' performance, we focused on two reward functions: reward rate (RR, defined as the average reward per second) and reward per trial (RTrial, defined as the average reward per trial) for a given reward context for each session. To estimate the reward functions in relation to *me* and *z* adjustments for a given reward context, we numerically obtained choice and RT values for different combinations of *z* (ranging from 0 to 1) and *me* (ranging from -0.6 to 0.6 coherence unless otherwise specified), given *a, k* and non-decision time values fitted by the full model. We then calculated RR and RTrial, using trial-matched parameters, including the actual ITI, timeout, and large:small reward ratio. RR_{max} and $RTrial_{max}$ were identified as the maximal values given the sampled *me-z* combinations, using 1000 trials for each coherence × direction condition. Optimal *me* and *z* adjustments were defined as the *me* and *z* values corresponding to RR_{max} or $RTrial_{max}$. $RR_{predict}$ and $RTrial_{predict}$ were calculated with the fitted *me* and *z* values in the full model.

Acknowledgments

We thank Takahiro Doi for helpful comments, Javier Caballero and Rachel Gates for animal training, Jean Zweigle for animal care, and Michael Yoder for data entry. This work was supported by the National Eye Institute Grant R01 EY-022411 (LD and JIG), the Penn Medicine Neuroscience Center Pilot Program (LD), and a Hearst Foundation Fellowship (YF).

Competing interests

The authors declare that no competing interests exist.

References

Ashby FG (1983) A Biased Random-Walk Model for 2 Choice Reaction-Times. Journal of Mathematical Psychology 27:277-297.

Barnard GA (1946) Sequential Tests in Industrial Statistics. J Roy Stat Soc B 8:1-26.

Bennur S, Gold JI (2011) Distinct representations of a perceptual decision and the associated oculomotor plan in the monkey lateral intraparietal area. J Neurosci 31:913-921.

Blank H, Biele G, Heekeren HR, Philiastides MG (2013) Temporal characteristics of the influence of punishment on perceptual decision making in the human brain. J Neurosci 33:3939-3952.

Bogacz R, Brown E, Moehlis J, Holmes P, Cohen JD (2006) The physics of optimal decision making: a formal analysis of models of performance in two-alternative forced-choice tasks. Psychol Rev 113:700-765.Churchland AK, Kiani R, Shadlen MN (2008) Decision-making with multiple alternatives. Nat Neurosci 11:693-702.

Churchland AK, Kiani R, Chaudhuri R, Wang XJ, Pouget A, Shadlen MN (2011) Variance as a signature of neural computations during decision making. Neuron 69:818-831.

Cicmil N, Cumming BG, Parker AJ, Krug K (2015) Reward modulates the effect of visual cortical microstimulation on perceptual decisions. eLife 4.

Connolly PM, Bennur S, Gold JI (2009) Correlates of perceptual learning in an oculomotor decision variable. J Neurosci 29:2136-2150.

Diederich A, Busemeyer JR (2006) Modeling the effects of payoff on response bias in a perceptual discrimination task: bound-change, drift-rate-change, or two-stage-processing hypothesis. Percept Psychophys 68:194-207.

Ding L (2015) Distinct dynamics of ramping activity in the frontal cortex and caudate nucleus in monkeys. J Neurophysiol 114:1850-1861.

Ding L, Gold JI (2010) Caudate encodes multiple computations for perceptual decisions. J Neurosci 30:15747-15759.

Ding L, Gold JI (2012a) Neural correlates of perceptual decision making before, during, and after decision commitment in monkey frontal eye field. Cereb Cortex 22:1052-1067.

Ding L, Gold JI (2012b) Separate, causal roles of the caudate in saccadic choice and execution in a perceptual decision task. Neuron 75:865-874.

Drugowitsch J, Moreno-Bote R, Churchland AK, Shadlen MN, Pouget A (2012) The cost of accumulating evidence in perceptual decision making. J Neurosci 32:3612-3628.

Frank MJ, Gagne C, Nyhus E, Masters S, Wiecki TV, Cavanagh JF and Badre D (2015) fMRI and EEG Predictors of Dynamic Decision Parameters during Human Reinforcement Learning. J Neurosci 35: 484-494.

Feng S, Holmes P, Rorie A, Newsome WT (2009) Can monkeys choose optimally when faced with noisy stimuli and unequal rewards? PLoS computational biology 5:e1000284.

Gao JA, Tortell R, McClelland JL (2011) Dynamic Integration of Reward and Stimulus Information in Perceptual Decision-Making. PLoS One 6.

Gigerenzer G (2010) Moral satisficing: rethinking moral behavior as bounded rationality. Topics in cognitive science 2:528-554.

Gigerenzer G, Goldstein DG (1996) Reasoning the fast and frugal way: Models of bounded rationality. Psychological Review 103:650-669.

Gigerenzer G, Gaissmaier W (2011) Heuristic Decision Making. Annual Review of Psychology 62:451-482.

Gold JI, Shadlen MN (2002) Banburismus and the brain: decoding the relationship between sensory stimuli, decisions, and reward. Neuron 36:299-308.

Gold JI, Shadlen MN (2007) The neural basis of decision making. Annu Rev Neurosci 30:535-574.

Goldfarb S, Leonard NE, Simen P, Caicedo-Nunez CH, Holmes P (2014) A comparative study of drift diffusion and linear ballistic accumulator models in a reward maximization perceptual choice task. Front Neurosci 8:148.

Goldstein DG, Gigerenzer G (2002) Models of ecological rationality: the recognition heuristic. Psychol Rev 109:75-90.

Goodrich MA, Stirling WC, Frost RL (1998) A theory of satisficing decisions and control. IEEE Transactions on Systems, Man, and Cybernetics - Part A: Systems and Humans 28:763-779.

Hanks TD, Ditterich J, Shadlen MN (2006) Microstimulation of macaque area LIP affects decision-making in a motion discrimination task. Nat Neurosci 9:682-689.

Hanks TD, Mazurek ME, Kiani R, Hopp E, Shadlen MN (2011) Elapsed decision time affects the weighting of prior probability in a perceptual decision task. J Neurosci 31:6339-6352.

Jones PR, Moore DR, Shub DE, Amitay S (2015) The Role of Response Bias in Perceptual Learning. J Exp Psychol Learn Mem Cogn. 41:1456–1470.

Kiani R, Shadlen MN (2009) Representation of confidence associated with a decision by neurons in the parietal cortex. Science 324:759-764.

Klein SA (2001) Measuring, estimating, and understanding the psychometric function: a commentary. Percept Psychophys 63:1421-1455.

Horwitz GD, Newsome WT (2001) Target selection for saccadic eye movements: Direction selective visual responses in the superior colliculus. J Neurophysiol. 86:2527-2542

Krajbich I, Armel C, Rangel A (2010) Visual fixations and the computation and comparison of value in simple choice. Nat Neurosci 13:1292-1298.

Latimer KW, Yates JL, Meister ML, Huk AC, Pillow JW (2015) Single-trial spike trains in parietal cortex reveal discrete steps during decision-making. Science 349:184-187.

Leite FP, Ratcliff R (2011) What cognitive processes drive response biases? A diffusion model analysis. Judgm Decis Mak 6:651-687.

Liston DB, Stone LS (2008) Effects of prior information and reward on oculomotor and

perceptual choices. J Neurosci 28:13866-13875.

Lo CC, Wang XJ (2006) Cortico-basal ganglia circuit mechanism for a decision threshold in reaction time tasks. Nat Neurosci 9:956-963.

Lo CC, Wang CT, Wang XJ (2015) Speed-accuracy tradeoff by a control signal with balanced excitation and inhibition. J Neurophysiol 114:650-661.

Maddox WT, Bohil CJ (1998) Base-rate and payoff effects in multidimensional perceptual categorization. Journal of experimental psychology Learning, memory, and cognition 24:1459-1482.

Matzke D, Wagenmakers EJ (2009) Psychological interpretation of the ex-Gaussian and shifted Wald parameters: a diffusion model analysis. Psychon Bull Rev 16:798-817.

Milosavljevic M, Malmaud J, Huth A, Koch C, Rangel A. (2001) The Drift Diffusion Model can account for the accuracy and reaction times of value-based choice under high and low time pressure. Judgment and Decision Making 5:437-449.

Mulder MJ, Wagenmakers EJ, Ratcliff R, Boekel W, Forstmann BU (2012) Bias in the brain: a diffusion model analysis of prior probability and potential payoff. J Neurosci 32:2335-2343.

Newsome WT, Britten KH, Movshon JA (1989) Neuronal correlates of a perceptual decision. Nature 341:52-54.

Nikolaev AR, Gepshtein S, van Leeuwen C (2016) Intermittent regime of brain activity at the early, bias-guided stage of perceptual learning. J Vis. 16(14):11.

Nomoto K, Schultz W, Watanabe T, Sakagami M (2010) Temporally extended dopamine responses to perceptually demanding reward-predictive stimuli. J Neurosci 30:10692-10702.

Nosofsky RM, Palmeri TJ (1997) An exemplar-based random walk model of speeded classification. Psychol Rev 104:266-300.

Oh H, Beck JM, Zhu P, Sommer MA, Ferrari S, Egner T (2016) Satisficing in split-second decision making is characterized by strategic cue discounting. Journal of Experimental Psychology: Learning, Memory, and Cognition 42:1937-1956.

Palmer J, Huk AC, Shadlen MN (2005) The effect of stimulus strength on the speed and accuracy of a perceptual decision. Journal of vision 5:376-404.

Rao RP (2010) Decision making under uncertainty: a neural model based on partially observable markov decision processes. Frontiers in computational neuroscience 4:146.

Ratcliff R (1978) Theory of Memory Retrieval. Psychological Review 85:59-108.

Ratcliff R, Tuerlinckx F (2002) Estimating parameters of the diffusion model: Approaches to dealing with contaminant reaction times and parameter variability. Psychon B Rev 9:438-481.

Ratcliff R, Cherian A, Segraves M (2003) A comparison of macaque behavior and superior colliculus neuronal activity to predictions from models of two-choice decisions. J Neurophysiol 90:1392-1407.

Ratcliff R, Smith PL (2004) A comparison of sequential sampling models for two-choice reaction time. Psychol Rev 111:333-367.

Ratcliff R, Van Zandt T, McKoon G (1999) Connectionist and diffusion models of reaction time. Psychological Review 106:261-300.

Roitman JD, Shadlen MN (2002) Response of neurons in the lateral intraparietal area during a combined visual discrimination reaction time task. J Neurosci 22:9475-9489.

Rorie AE, Gao J, McClelland JL, Newsome WT (2010) Integration of sensory and reward information during perceptual decision-making in lateral intraparietal cortex (LIP) of the macaque monkey. PLoS One. 5:e9308.

Sakawa M, Yauchi K (2001) An interactive fuzzy satisficing method for multiobjective nonconvex programming problems with fuzzy numbers through coevolutionary genetic algorithms. IEEE transactions on systems, man, and cybernetics Part B, Cybernetics : a publication of the IEEE Systems, Man, and Cybernetics Society 31:459-467.

Serences JT (2008) Value-based modulations in human visual cortex. Neuron 60:1169-1181.

Shadlen MN, Newsome WT (2001) Neural basis of a perceptual decision in the parietal cortex (area LIP) of the rhesus monkey. J Neurophysiol. 86:1916-36.

Shadlen MN, Shohamy D (2016) Decision Making and Sequential Sampling from Memory. Neuron. 90:927-939.

Simen P, Contreras D, Buck C, Hu P, Holmes P, Cohen JD (2009) Reward rate optimization in two-alternative decision making: empirical tests of theoretical predictions. Journal of experimental psychology Human perception and performance 35:1865-1897.

Simon HA (1956) Rational choice and the structure of the environment. Psychol Rev 63:129-138.

Simon HA (1966) Theories of Decision-Making in Economics and Behavioural Science. In: Surveys of Economic Theory: Resource Allocation, pp 1-28. London: Palgrave Macmillan UK.

Simon HA (1982) Models of bounded rationality. Cambridge, Mass.: MIT Press.

Smith PL, Ratcliff R (2004) Psychology and neurobiology of simple decisions. Trends in Neurosciences 27:161-168.

Stirling WC (2003) Satisficing games and decision making : with applications to engineering and computer science. Cambridge, England ; New York: Cambridge University Press.

Summerfield C, Koechlin E (2010) Economic value biases uncertain perceptual choices in the parietal and prefrontal cortices. Frontiers in Human Neuroscience 4.

Sutton RS, Barto A (1998) Reinforcement learning: An introduction. Cambridge, Massachusetts, USA; MIT Press.

Teichert T, Ferrera VP (2010) Suboptimal integration of reward magnitude and prior reward likelihood in categorical decisions by monkeys. Front Neurosci 4:186.

Thura D, Beauregard-Racine J, Fradet CW, Cisek P (2012) Decision making by urgency gating: theory and experimental support. J Neurophysiol 108:2912-2930.

Vandekerckhove J, Tuerlinckx F (2007) Fitting the Ratcliff diffusion model to

experimental data. Psychon B Rev 14:1011-1026.

Voss A, Rothermund K, Voss J (2004) Interpreting the parameters of the diffusion model: an empirical validation. Mem Cognit 32:1206-1220.

Wald A (1947) Sequential analysis. New York: Wiley.

Wald A, Wolfowitz J (1948) Optimum Character of the Sequential Probability Ratio Test. Ann Math Stat 19:326-339.

Wang AY, Miura K, Uchida N (2013) The dorsomedial striatum encodes net expected return, critical for energizing performance vigor. Nat Neurosci 16:639-647.

Wei W, Rubin JE, Wang XJ (2015) Role of the indirect pathway of the basal ganglia in perceptual decision making. J Neurosci 35:4052-4064.

White CN, Poldrack RA (2014) Decomposing bias in different types of simple decisions. Journal of experimental psychology Learning, memory, and cognition 40:385-398.

Wiecki TV, Sofer I, Frank MJ (2013) HDDM: Hierarchical Bayesian estimation of the Drift-Diffusion Model in Python. Frontiers in neuroinformatics 7:14.

Wierzbicki AP (1982) A mathematical basis for satisficing decision making. Mathematical Modelling 3:391-405.

Zacksenhouse M, Bogacz R, Holmes P (2010) Robust versus optimal strategies for two-alternative forced choice tasks. Journal of Mathematical Psychology 54:230-246.

Zylberberg A, Fetsch CR, Shadlen MN (2016) The influence of evidence volatility on choice, reaction time and confidence in a perceptual decision. eLife 5.

Figure legends

Figure 1. Theoretical framework and task design.

A, Schematics of the drift-diffusion model (DDM). Motion evidence is modeled as samples from a unit-variance Gaussian distribution (mean: signed coherence, *Coh*). Effective evidence is modeled as the sum of motion evidence and an internal momentary-evidence bias (*me*). The decision variable starts at value $a \times z$, where z governs decision-rule bias, and accumulates effective evidence over time with a proportional scaling factor (k). A decision is made when the decision variable reaches either bound. Reaction time (RT) is assumed to be the sum of the decision time and a saccade-specific non-decision time.

B, Reaction-time (RT) random-dot visual motion direction discrimination task with asymmetric rewards. A monkey makes a saccade decision based on the perceived global motion of a random-dot kinematogram. Reward is delivered on correct trials and with a magnitude that depends on reward context. Two reward contexts (LR-Left and LR-Right) were alternated in blocks of trials with signaled block changes. Motion directions and strengths were randomly interleaved within blocks.

Figure 2. Relationships between sensitivity and bias from logistic fits to choice data.

A, For each monkey, the probability of making a rightward choice is plotted as a function of signed coherence (–/+ indicate left/right motion) from all sessions, separately for the two reward contexts, as indicated. Lines are logistic fits.

B, Top row: Motion sensitivity (steepness of the logistic function) in each context as a function of session index (colors as in A). Solid lines indicate significant positive partial Spearman correlation after accounting for changes in reward ratio across sessions ($p<0.05$). Black dashed lines indicate each monkey's motion sensitivity in the same task with equal rewards before training on this asymmetric reward task. Middle row: ΔBias (horizontal shift between the two psychometric functions in the two reward contexts at chance level) as a function of session index. Solid line indicates significant negative partial Spearman correlation after accounting for changes in reward ratio across sessions ($p<0.05$). Bottom row: Lapse rate as a function of session index (median=0 for all three monkeys).

C, ΔBias as a function of motion sensitivity for each reward context (colors as in A). Solid line indicates a significant negative partial Spearman correlation after accounting for changes in reward ratio across sessions ($p<0.05$).

D, Optimal versus fitted Δbias. Optimal Δbias was computed as the difference in the horizontal shift in the psychometric functions in each reward context that would have resulted in the maximum reward per trial, given each monkey's fitted motion sensitivity

and experienced values of reward ratio and coherences from each session (see Fig. S2a). Solid lines indicate significant negative Spearman correlation ($p<0.01$). Partial Spearman correlation after accounting for changes in reward ratio across sessions are also significant for money F and C ($p<0.01$).

Figure 3. Comparison of choice and RT data to HDDM fits with both momentary-evidence (*me*) and decision-rule (*z*) biases.

A, Psychometric data (points as in Fig. 2A) shown with predictions based on HDDM fits to both choice and RT data.

B, RT data (circles) and HDDM-predicted RT distributions (lines). Both sets of RT data were plotted as values corresponding to the 20th, 40th, 60th, and 80th percentiles of the full distribution. Top row: Trials in which monkey chose the left target. Bottom row: Trials in which monkeys chose the right target. Columns correspond to each monkey (as in A), divided into choices in the large- (left column) or small- (right column) reward direction (correct/error choices are as indicated in the left-most columns; note that no reward was given on error trials). The HDDM-predicted RT distributions were generated with 50 runs of simulations, each run using the number of trials per condition (motion direction $\times$ coherence $\times$ reward context $\times$ session) matched to experimental data and using the best-fitting HDDM parameters for that monkey.

Figure 4. Actual versus optimal adjustments of momentary-evidence (*me*) and decision-rule (*z*) biases.

A, Schematic of the comparison procedure. Choice and RT data from the two reward contexts in a given session were fitted separately using the HDDM. These context- and session-specific best-fitting *me* and *z* values are plotted as the monkey's data (black circles in *B* and *C*). Optimal values were determined by taking the best-fitting values of parameters *a, k,* and non-decision times from the HDDM fits, then sampling *me* and *z* uniformly over broad ranges to predict choice and RT behavior. For each *me* and *z* combination, the predicted probability of left/right choice and RTs were used with actual task information (inter-trial interval, error timeout and reward sizes) to calculate the expected reward rate (RR) and average reward per trial (RTrial). Optimal *me*/*z* adjustments were then identified to maximize RR (purple) or RTrial (orange).

B, Scatterplots of the monkeys' *me*/*z* adjustments (black), predicted optimal adjustments for maximal RR (purple), and predicted optimal adjustments for maximal RTrial (orange), for the two reward contexts in all sessions (each data point was from a single session). Values of $me>0$ or $z>0.5$ produce biases favoring rightward choices.

C, Scatterplots of the differences in *me* (abscissa) and *z* (ordinate) between the two reward contexts for monkeys (black), for maximizing RR (purple), and for maximizing

RTrial (orange). Positive Δme and Δz values produce biases favoring large-reward choices.

Figure 5. Predicted versus optimal reward per trial (RTrial).

A, Scatterplots of $RTrial_{predict}$:$RTrial_{max}$ ratio as a function of session index. Each session was represented by two ratios, one for each reward context. Mean ratio across contexts and sessions: 0.977 for monkey F, 0.984 for monkey C, and 0.983 for monkey A.

B, 97% $RTrial_{max}$ contours for all sessions, computed using the best-fitting HDDM parameters and experienced coherences and reward ratios from each session. Light grey: LR-Left blocks; Dark grey: LR-Right blocks.

C, The monkeys' adjustments (blue in LR-Left blocks, red in LR-Right blocks) were largely within the 97% $RTrial_{max}$ contours for all sessions and tended to cluster in the *me* over-biased, *z* under-biased quadrants (except Monkey F in the LR-Right blocks). The contours and monkeys' adjustments are centered at the optimal adjustments for each session.

Figure 6. Relationships between adjustments of momentary-evidence (*me*) and decision-rule (*z*) biases and RTrial function properties.

A, Mean RTrial as a function of *me* and *z* adjustments for the LR-Left (top) and LR-Right (bottom) blocks. RTrial was normalized to $RTrial_{max}$ for each session and then averaged across sessions.

B, Scatterplot of the total variance in *me* and *z* adjustments across sessions (ordinate) and the area of ≥97% max of the average RTrial patch (abscissa). Variance and patch areas were measured separately for the two reward blocks (circles for LR-Left blocks, squares for LR-Right blocks).

C, D, The monkeys' session- and context-specific values of *me* (C) and *z* (D) co-varied with the orientation of the >97% heatmap patch (same as the contours in Fig. 5B). Orientation is measured as the angle of the tilt from vertical. Circles: data from LR-Left block; squares: data from LR-Right block; lines: significant correlation between *me* (or *z*) and patch orientations across monkeys (p<0.05). Colors indicate different monkeys (see legend in B).

E, Scatterplots of conditionally optimal versus fitted Δme (top row) and Δz (bottom row). For each reward context, the conditionally optimal *me (z)* value was identified given the monkey's best-fitting z (*me*) values. The conditionally optimal Δme *(*Δz*)* was the difference between the two conditional optimal *me (z)* values for the two reward contexts. Grey lines indicate the range of conditional Δme (Δz) values corresponding to the 97%

maximal RTrial given the monkeys' fitted z (*me*) values.

Figure 7. Relationships between starting and ending values of the satisficing, reward function gradient-based updating process.

Example gradient lines of the average RTrial maps for the three monkeys are color coded based on the end point of gradient-based *me* and *z* adjustments in the following ways: 1) *me* biases to large reward whereas *z* biases to small reward (magenta); 2) *z* biases to large reward whereas *me* biases to small reward (blue); 3) *me* and *z* both bias to large reward (green), and 4) *me* and *z* both bias to small reward (yellow). The gradient lines ended on the 97% $RTrial_{max}$ contours. Top row: LR-Left block; bottom row: LR-Right block.

Figure 8. The satisficing reward function gradient-based model.

A, Illustration of the procedure for predicting a monkey's *me* and *z* values for a given RTrial function. For better visibility, RTrial for the LR-Left reward context in an example session is shown as a heatmap in greyscale. Gradient lines are shown as black lines. The square indicates the unbiased *me* and *z* combination (average values across the two reward contexts). The four trajectories represent gradient-based searches based on four alternative assumptions of initial values (see table on the right). Open circles indicate the end values. Grey filled circle indicates the monkey's actual *me* and z. Note that the end points differ among the four assumptions, with the magenta circle being the closest to the monkey's fitted *me* and *z* of that session.

B, Scatterplots of the predicted and actual Δ*me* and Δz between reward contexts. Grey circles here are the same as the black circles in Fig. 4C. Colors indicate model identity, as in A.

C, Average regression coefficients between each monkey's Δ*me* (left four bars) and Δ*z* (right four bars) values and predicted values for each of the four models. Filled bars: *t*-test, $p < 0.05$.

D, Covariation of *me* (top) and *z* (bottom) with the orientation of the >97% RTrial heatmap patch for monkeys and predictions of the four models. Blue: data from LR-Left blocks, red: data from LR-Right blocks. Data in the "Monkey" column are the same as in Fig 6C and D. Note that predictions of the "over-*me*" model best matched the monkey data than the other models.

Supplementary Figure legends

Figure S1. Logistic regression fits.

A, Choice data from example sessions for each of the three monkeys, plotted as in Fig. 2A. Lines: fits with logistic regressions.

B, Scatterplots of mean likelihood per trial, assuming binomial errors. Red circles indicate the sessions shown in A.

Figure S2.

A, Identification of the optimal ∆bias for an example session using logistic fits. For each reward context (blue for LR-Left and red for LR-Right), RTrial was computed as a function of bias values sampled uniformly over a broad range, given the session-specific sensitivities, lapse rate, coherences and large:small reward ratio. The optimal ∆bias was defined as the difference between the bias values with the maximal RTrial for the two reward contexts. The fitted ∆bias was defined as the difference between the fitted bias values for the two reward contexts.

B, The optimal bias decreases with increasing sensitivity. The example heatmap shows normalized RTrial as a function of sensitivity and bias values in the LR-Right blocks, assuming the same coherence levels as used for the monkeys and a large:small reward ratio of 2.3. The black curve indicates the optimal bias values for a given sensitivity value.

C, Scatterplots of optimal ∆biases obtained via the procedure described above as a function of sensitivity for each of the two reward contexts. Same format as Figure 3B. Solid lines indicate significant partial Spearman correlation after accounting for changes in reward ratio across sessions ($p<0.05$). Note that the scatterplots of the monkeys' ∆biases and sensitivities in Fig. 2C also show negative correlations, similar to this pattern.

Figure S3. Qualitative comparison between the monkeys' RT distribution and DDM predictions.

A, RT distributions as predicted by a DDM with no bias in decision rule (z) or momentary evidence (me; left), with $me>0$ (middle), and with $z>0.5$ (right). RT distributions are shown separately for correct (red) and error (black) trials and using values corresponding to 20th, 40th, 60th, and 80th percentiles. Positive/negative coh values indicate rightward/leftward saccades. The values of me and z were chosen to induce similar choice biases (~0.075 in coherence units). Note that the me bias induces large asymmetries in RT both between the two choices and between correct and error trials, whereas the z bias induces a large asymmetry in RT for the two choices, but with little

asymmetry between correct and error trials.

B, The monkeys' mean RTs for four quantiles for the LR-Right (*top*) and LR-Left (*bottom*) reward contexts, respectively (same convention as in A). Note the presence of substantial asymmetries between correct and error trials for all three monkeys.

Figure S4. Fits to a DDM with collapsing bounds.

A, B, A DDM with collapsing bounds and both momentary evidence (*me*) and decision-rule (*z*) biases fit to each monkey's RT data. Same format as Fig. 3.

C, The model that included both *me* and *z* adjustments ("full") had smaller Akaike Information Criterion (AIC) values than reduced models ("me" or "z" only) across sessions. Note also the different ranges of ΔAIC for the full–*me* and full–z comparisons. The mean $\Delta AIC_{full\text{-}me}$ and $\Delta AIC_{full\text{-}z}$ values are significantly different from zero (Wilcoxon signed rank test, p=0.0007 for Monkey F's full–*me* comparison and p<0.0001 for all others).

D, RT distributions as predicted by the DDM with collapsing bounds, using no bias in *z* or *me* (*left*), *me*>0 (*middle*), or *z*>0.5 (*right*). Same format as Fig. S2A.

Figure S5. Estimates of momentary-evidence (*me*) and decision-rule (*z*) biases using the collapsing-bound DDM fits. Same format as Fig. 4B and C, except here only showing fits to the monkeys' data. As with the model without collapsing bounds, the adjustments in *me* tended to favor the large reward but the adjustments in *z* tended to favor the small reward.

Figure S6. Predicted versus optimal reward rate (RR). Same format as Fig. 5. Mean $RR_{predict}$:RR_{max} ratio across sessions=0.970 for monkey F, 0.980 for monkey C, and 0.979 for monkey A.

Figure S7. Correlation between fitted and conditionally optimal adjustments was stronger for matched sessions than for unmatched sessions. A, C: Momentary-evidence (Δ*me*) adjustments. B, D: Decision-rule (Δ*z*) adjustments. A, B: optimal values obtained with the RTrial function. C, D: optimal values obtained with the RR function. Red lines indicate the partial Spearman correlation coefficients between the fitted and optimal Δ*me* or Δ*z* (obtained in the same way as data in Fig. 6E) for matched sessions. Bars represent the histograms of partial correlation for unmatched sessions, which were obtained by 100 random shuffles of the sessions). Note that the correlation values for unmatched sessions were lower than those for matched sessions (Wilcoxson rank-sum

test, $p<0.001$ for all three monkeys and both Δme and Δz).

Figure S8. The monkeys' momentary-evidence (*me*) and decision-rule (*z*) adjustments reflected RR function properties. Same format as Fig. 6, but using RR instead of RTrial.

Figure S9: The HDDM model fitting procedure does not introduce spurious correlations between patch orientation and *me* value. Artificial sessions were simulated with fixed *me* values (±0.1 for the two reward contexts) and different *k* values. A: Recovered *k* values from HDDM fitting closely matched *k* values used for the simulations. B: Recovered *me* values from HDDM fitting closely matched *me* values used for simulation and did not correlate with RTrial patch orientation.

Figure S10. RR gradient trajectories color-coded by the end points of the *me/z* patterns. Same format as Fig. 7 but using gradients based on RR instead of RTrial.

Figure S11. Predictions of a RR gradient-based model. Same format as Fig. 8 but using gradients based on RR instead of RTrial.

Figure S12. Dependence of the orientation and area of the near-optimal RTrial patch on parameters reflecting internal decision process and external task specifications.

The top four rows show the RTrial heatmaps with two values of a single parameter indicated above, while keeping the other parameters fixed at the baseline values. The third and fourth rows show the estimated orientation (the slope value from a linear regression analysis) and area (in pixels), respectively, of the image patches corresponding to ≥97% of $RTrial_{max}$. The baseline values of the parameters are: *a*=1.5, *k*=6, non-decision times=0.3 sec for both choices, *ITI*=4 sec, *Timeout*=8 sec, *large-reward (LR): small-reward (SR) ratio*=2.

Supplementary Table 1.

Best-fitting parameters of HDDM.

	Monkey F (26079 trials)				Monkey C (37161 trials)				Monkey A (21089 trials)			
	LR-Left		LR-Right		LR-Left		LR-Right		LR-Left		LR-Right	
	Mean	Std	Mean	Std	Mean	Std	Mean	Std	Mean	Std	Mean	Std
a	1.67	0.16	1.43	0.12	1.77	0.09	1.53	0.13	1.33	0.13	1.36	0.09
k	10.22	1.87	9.91	2.11	6.58	0.51	5.08	0.92	4.04	0.33	3.45	0.46
t_1	0.31	0.03	0.29	0.03	0.35	0.04	0.33	0.05	0.29	0.04	0.27	0.04
t_0	0.28	0.04	0.31	0.05	0.33	0.04	0.31	0.03	0.21	0.08	0.26	0.04
z	0.6	0.03	0.57	0.04	0.62	0.03	0.2	0.04	0.57	0.06	0.39	0.04
me	-0.06	0.04	0.08	0.05	-0.14	0.04	0.21	0.06	-0.22	0.05	0.27	0.09

Supplementary Table 2.

The difference in deviance information criterion (ΔDIC) between the full model (i.e., the model that includes both *me* and *z*) and either reduced model (*me*-only or *z*-only), for experimental data and data simulated using each reduced model. Negative values favor the full model. Positive values favor the reduced models. Note that the ΔDIC for the experimental data deviated substantially - toward the negative direction - from the ΔDIC for the simulated data.

	Experimental Data				Simu: *me* model		Simu: *z* model	
	ΔDIC: full–*me*		ΔDIC: full–*z*		ΔDIC: full–*me*		ΔDIC: full–*z*	
	Mean	Std	Mean	Std	Mean	Std	Mean	Std
Monkey F	-124.6	2.7	-2560.4	3.9	3.1	8.7	0.2	10.5
Monkey C	-1700.4	2.4	-6937.9	0.9	17.5	10.1	1.8	1.2
Monkey A	-793.6	2.7	-2225.7	3.1	25.4	8.0	1.2	3.1

Figure 1

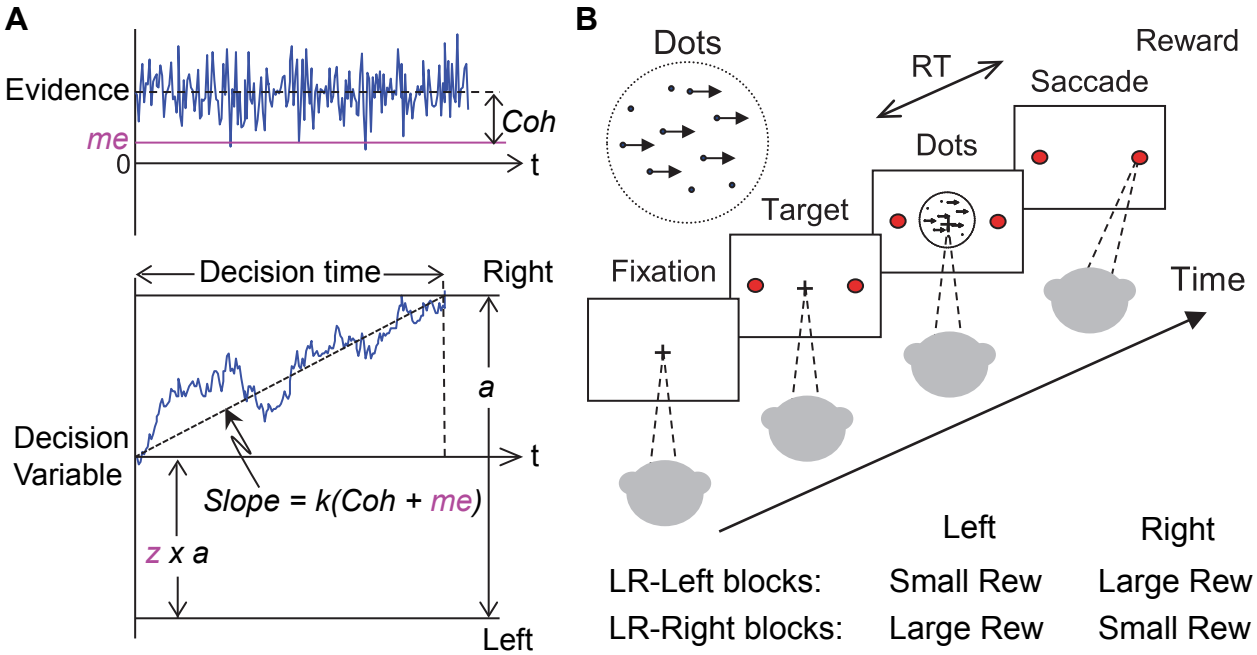
A
Evidence
me
0
Coh
t
Decision time
Right
a
Decision
Variable
t
Slope = k(Coh + me)
z x a
Left
B
Dots
RT
Reward
Saccade
Dots
Target
Fixation
Time
Left
Right
LR-Left blocks:
Small Rew
Large Rew
LR-Right blocks:
Large Rew
Small Rew

Figure 2

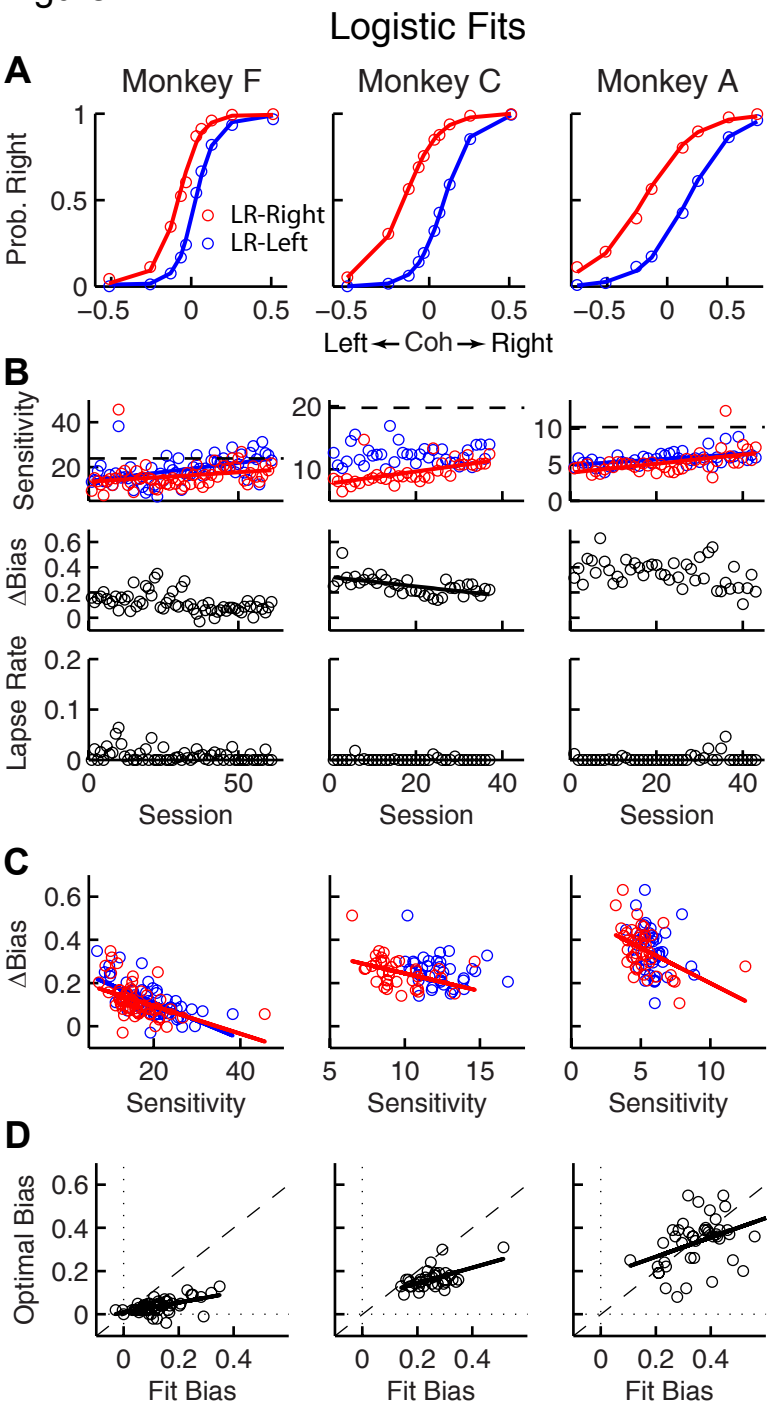
Logistic Fits
A
Monkey F
Monkey C
Monkey A
Prob. Right
LR-Right
LR-Left
Left ← Coh → Right
B
Sensitivity
ΔBias
Lapse Rate
Session
C
ΔBias
Sensitivity
D
Optimal Bias
Fit Bias

Figure 3

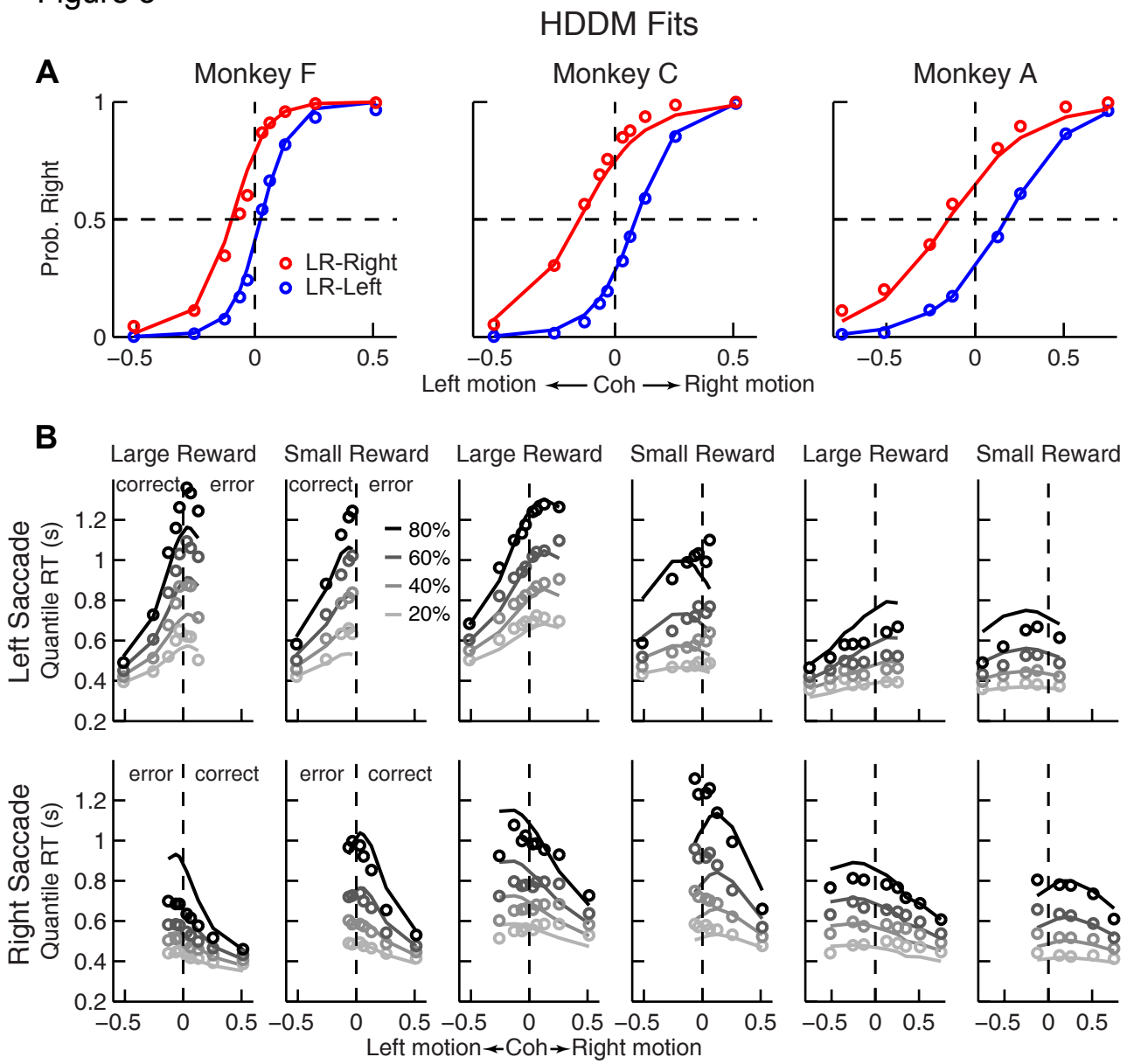
HDDM Fits
A
Monkey F
Monkey C
Monkey A
Prob. Right
LR-Right
LR-Left
Left motion ← Coh → Right motion
B
Large Reward
Small Reward
correct
error
80%
60%
40%
20%
Left Saccade
Quantile RT (s)
Right Saccade
Quantile RT (s)
Left motion ← Coh → Right motion

Figure 4

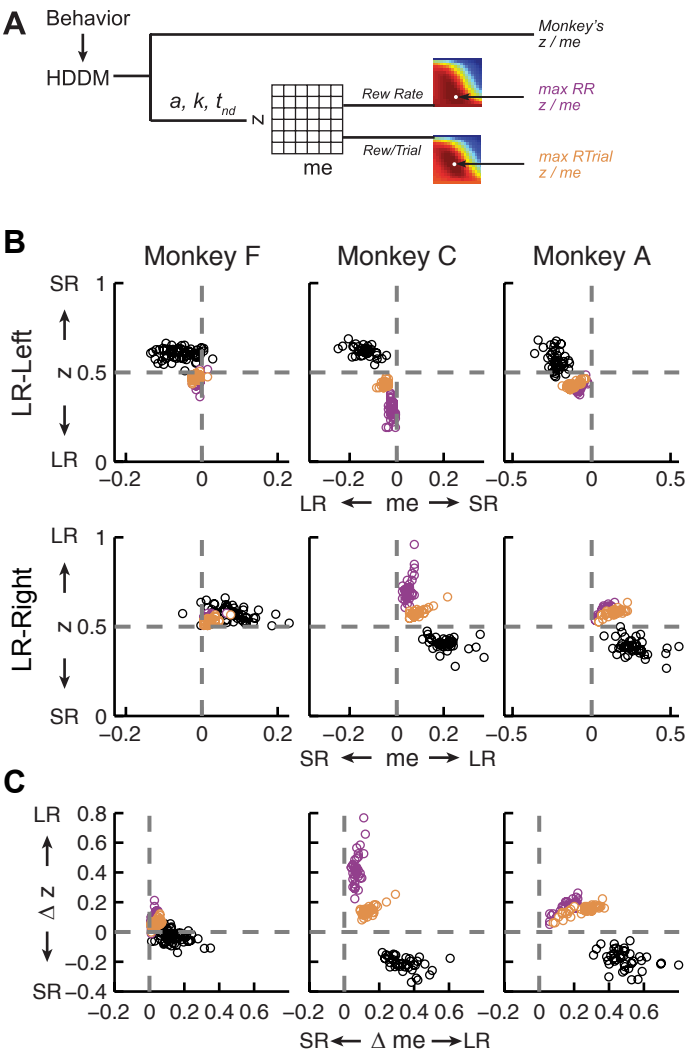
A
Behavior
HDDM
a, k, t_nd
z
me
Rew Rate
Rew/Trial
Monkey's z / me
max RR z / me
max RTrial z / me
B
Monkey F
Monkey C
Monkey A
LR-Left
LR-Right
SR
LR
z
me
C
Δ z
Δ me

Figure 5

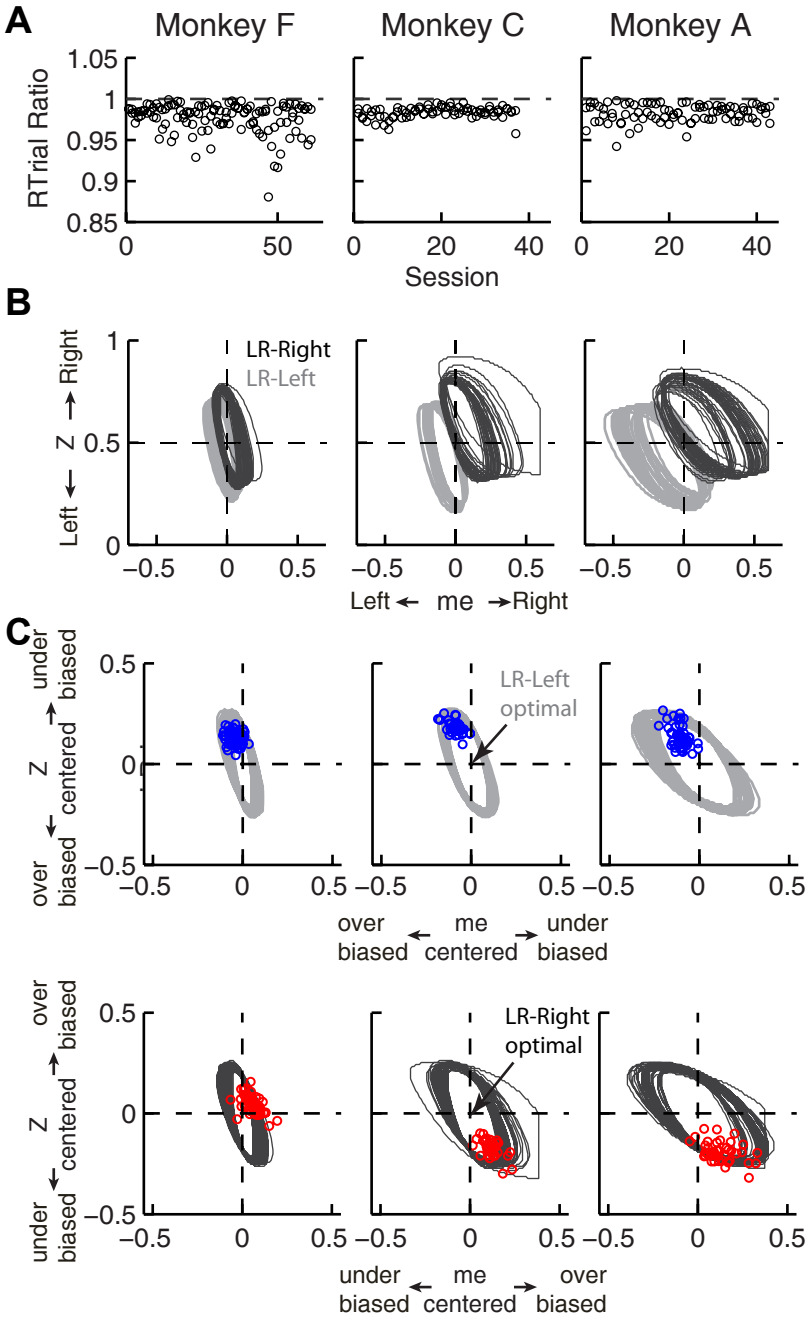
A
Monkey F
Monkey C
Monkey A
RTrial Ratio
1.05
1
0.95
0.9
0.85
0
50
0
20
40
0
20
40
Session
B
LR-Right
LR-Left
Left ← Z → Right
1
0.5
0
−0.5
0
0.5
Left ← me → Right
C
under biased
over biased
Z
0.5
0
−0.5
LR-Left optimal
over biased ← me centered → under biased
over biased
under biased
LR-Right optimal
under biased ← me centered → over biased

Figure 6

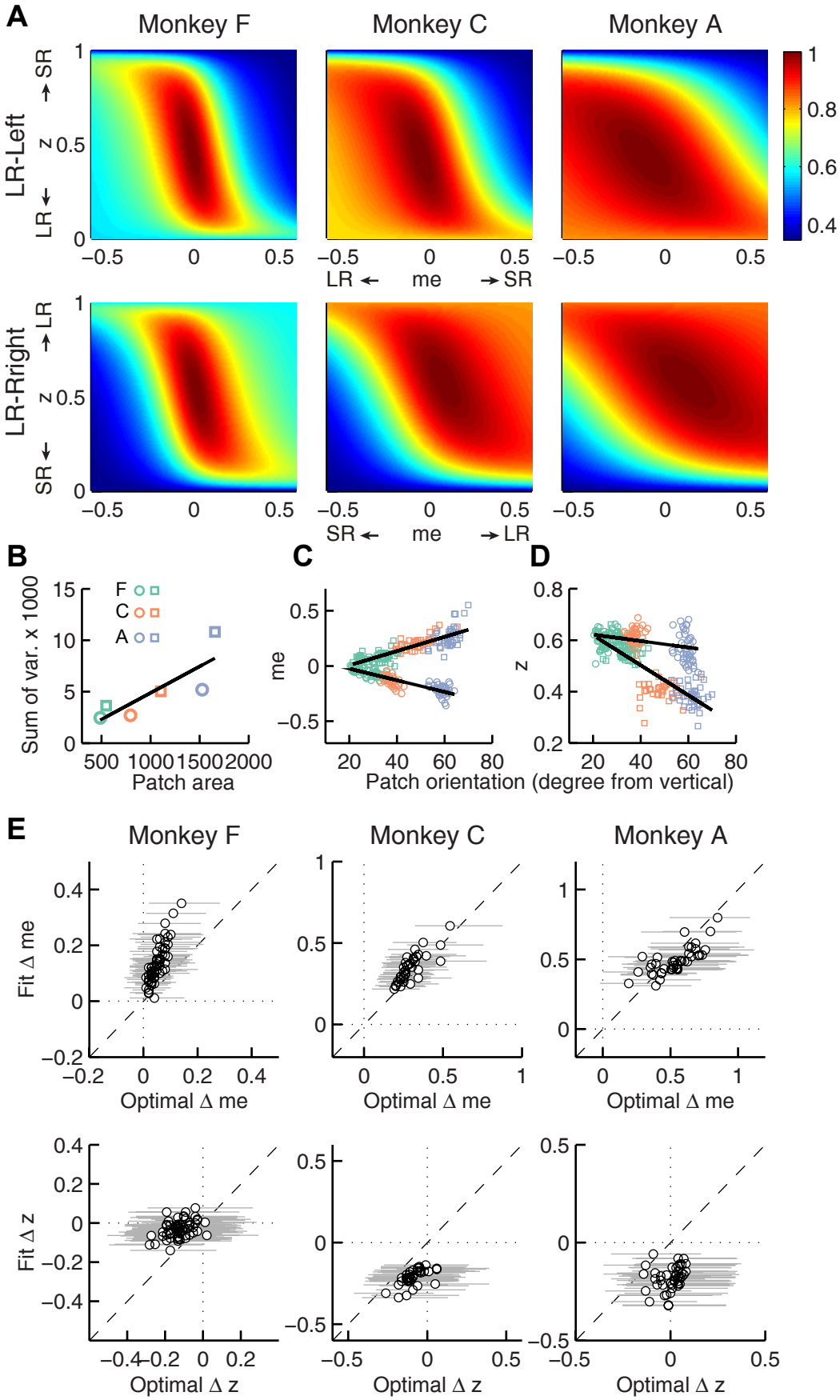

A
Monkey F
Monkey C
Monkey A
LR-Left
LR ← z → SR
LR ← me → SR
LR-Rright
SR ← z → LR
SR ← me → LR
B
Sum of var. x 1000
Patch area
F
C
A
C
me
D
z
Patch orientation (degree from vertical)
E
Monkey F
Monkey C
Monkey A
Fit Δ me
Optimal Δ me
Fit Δ z
Optimal Δ z

Figure 7

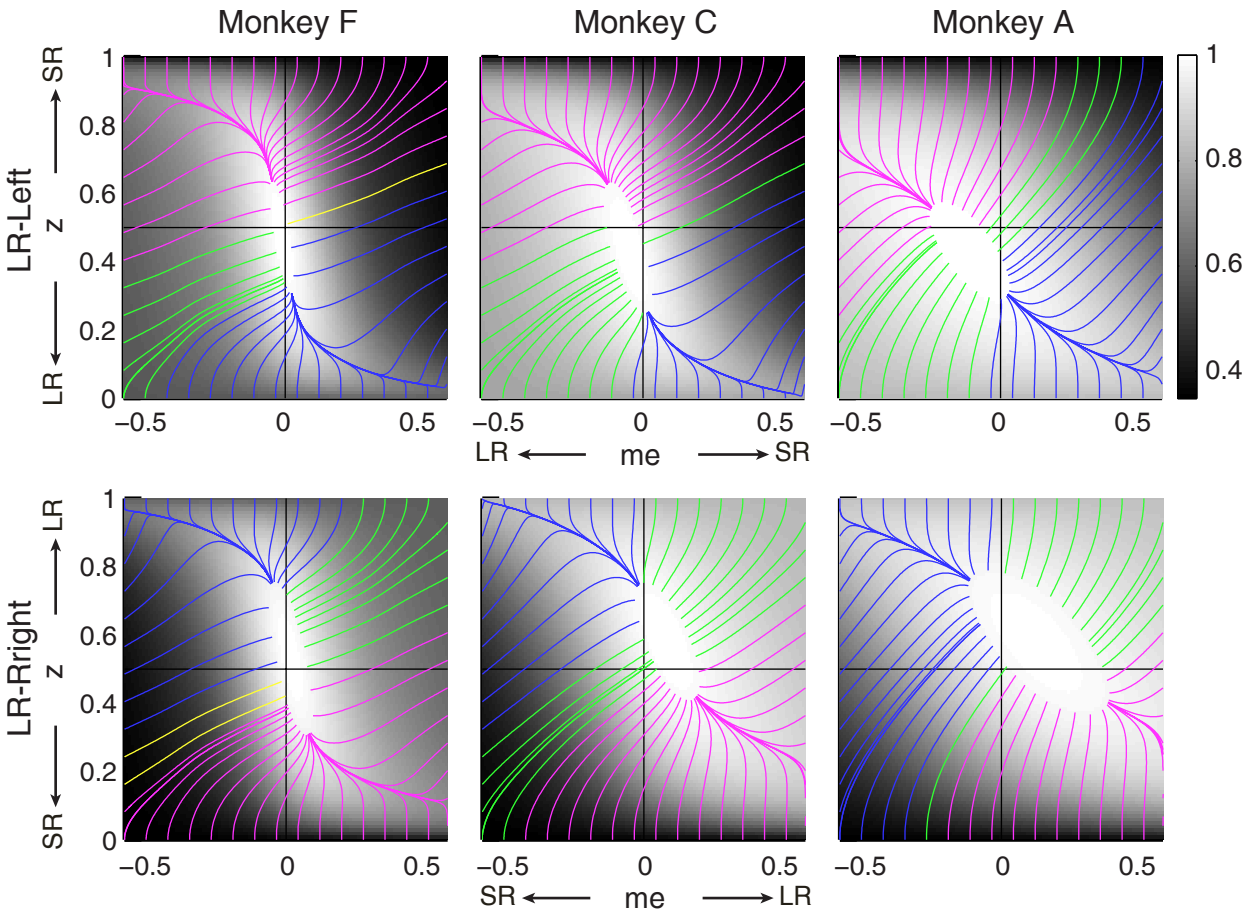

Trajectory end-point	me	z
	Over biased	Under biased
	Under biased	Over biased
	Over biased	Over biased
	Under biased	Under biased

Figure 8

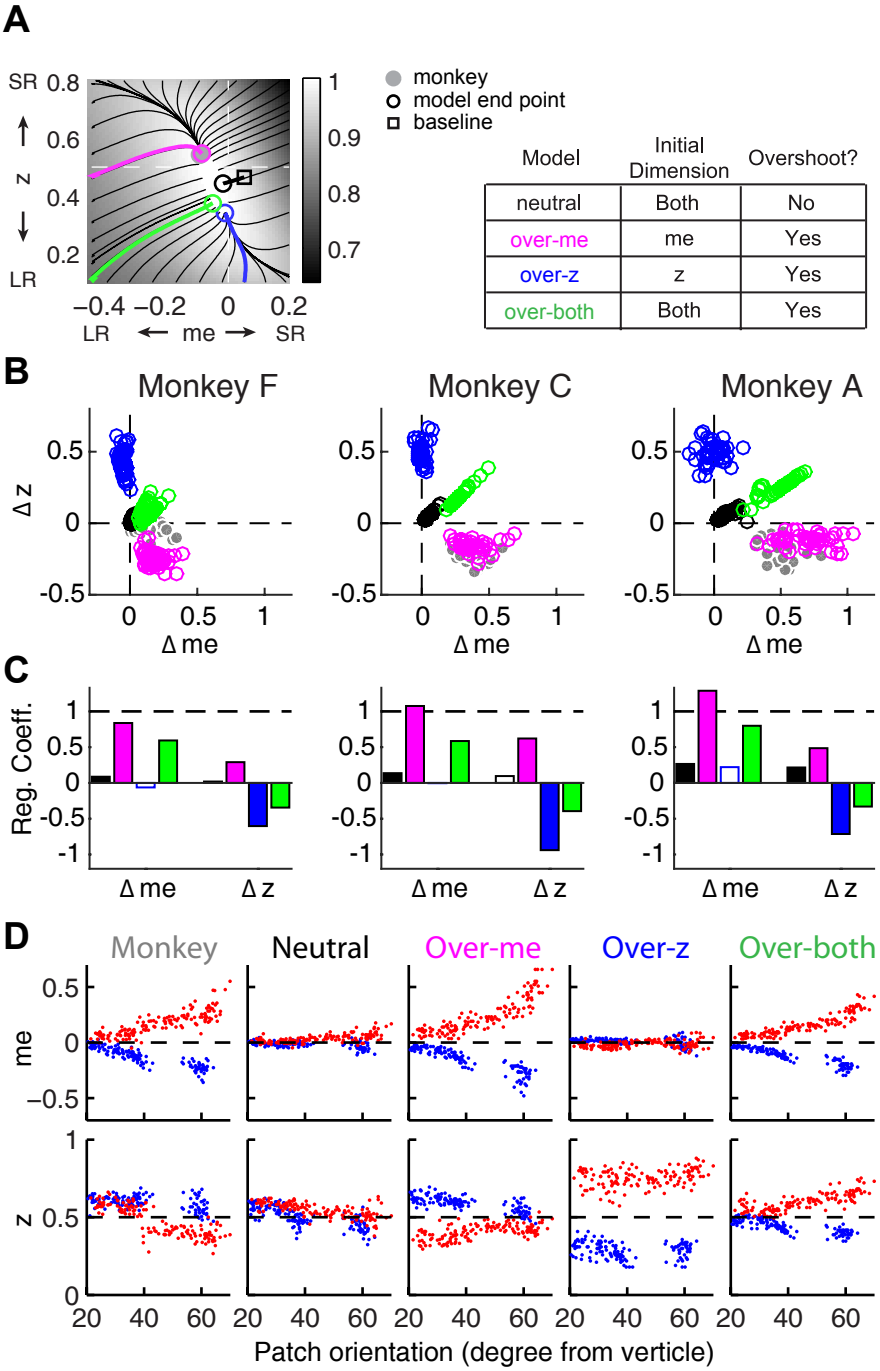

Model	Initial Dimension	Overshoot?
neutral	Both	No
over-me	me	Yes
over-z	z	Yes
over-both	Both	Yes

Figure S1

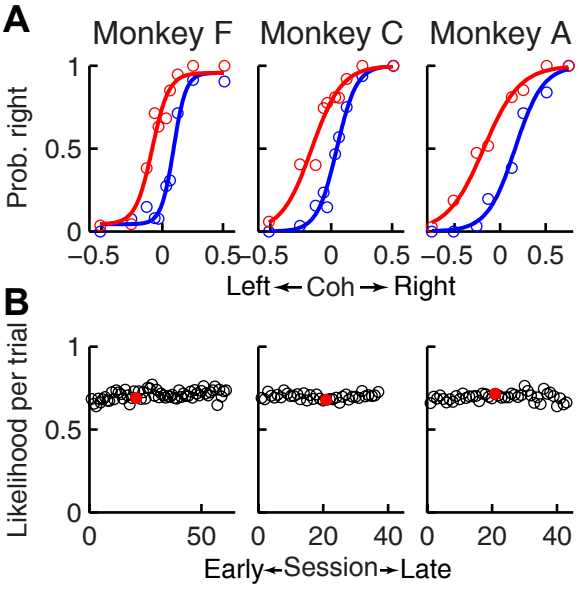
A
Monkey F
Monkey C
Monkey A
Prob. right
1
0.5
0
−0.5
0
0.5
Left ← Coh → Right
B
Likelihood per trial
1
0.5
0
0
50
0
20
40
0
20
40
Early ← Session → Late

Figure S2

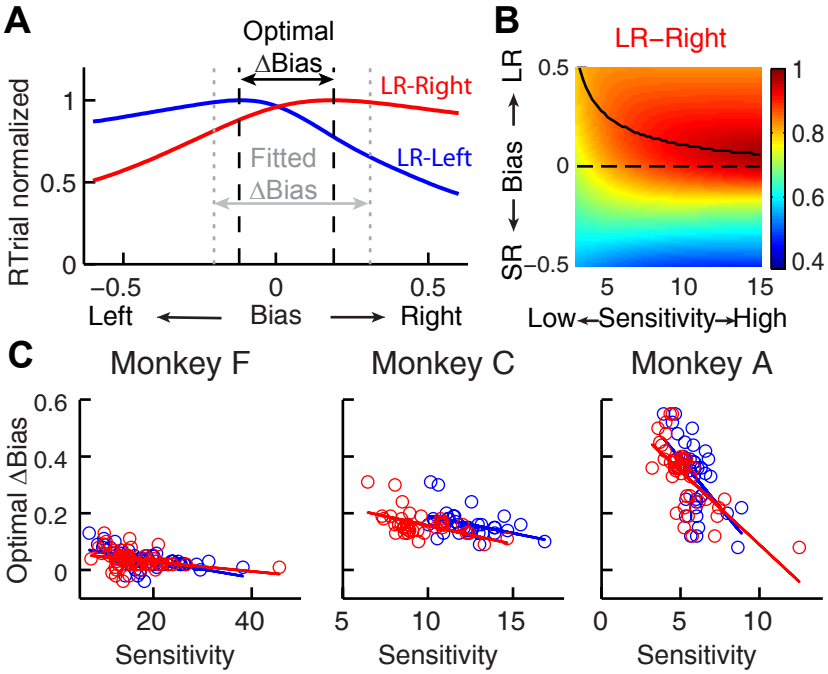
A
Optimal
ΔBias
LR-Right
LR-Left
Fitted
ΔBias
RTrial normalized
1
0.5
0
−0.5
0
0.5
Left
Bias
Right
B
LR−Right
LR
Bias
SR
0.5
0
−0.5
5
10
15
Low←Sensitivity→High
1
0.8
0.6
0.4
C
Monkey F
Monkey C
Monkey A
Optimal ΔBias
0.6
0.4
0.2
0
20
40
5
10
15
0
5
10
Sensitivity
Sensitivity
Sensitivity

Figure S3

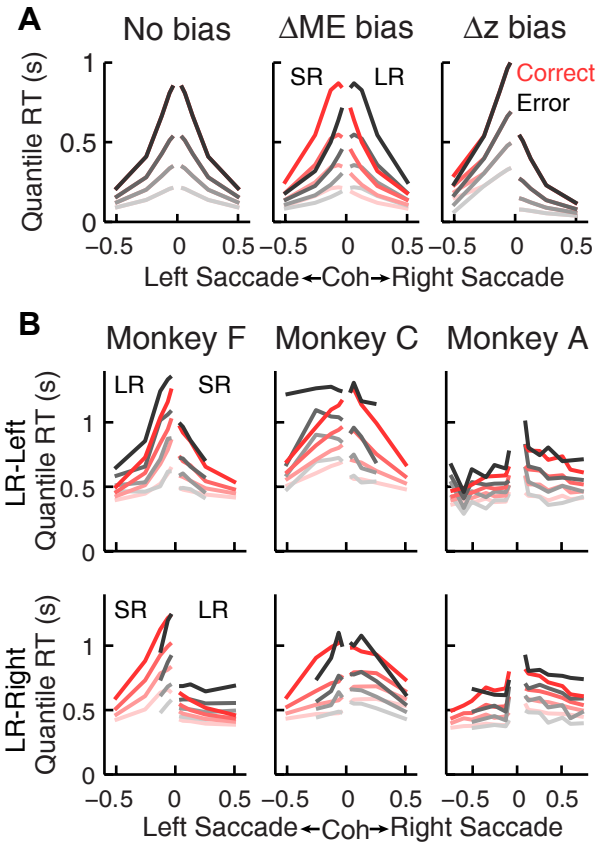
A
No bias
ΔME bias
Δz bias
Quantile RT (s)
SR
LR
Correct
Error
Left Saccade ← Coh → Right Saccade
B
Monkey F
Monkey C
Monkey A
LR-Left Quantile RT (s)
LR-Right Quantile RT (s)
Left Saccade ← Coh → Right Saccade

Figure S4

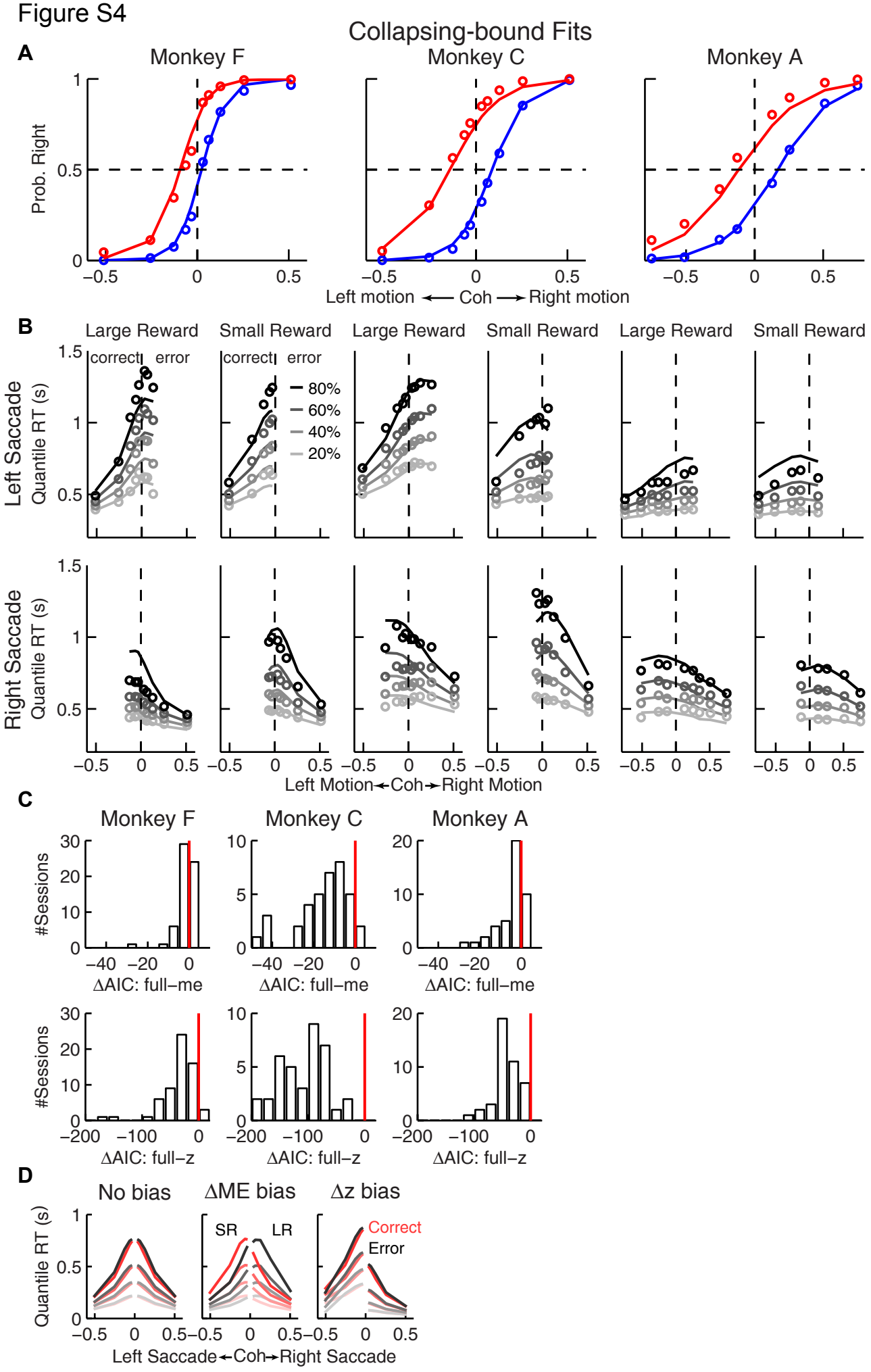
Collapsing-bound Fits
A
Monkey F
Monkey C
Monkey A
Prob. Right
Left motion ← Coh → Right motion
B
Large Reward
Small Reward
correct
error
80%
60%
40%
20%
Left Saccade Quantile RT (s)
Right Saccade Quantile RT (s)
Left Motion ← Coh → Right Motion
C
#Sessions
ΔAIC: full−me
ΔAIC: full−z
D
No bias
ΔME bias
Δz bias
SR
LR
Correct
Error
Quantile RT (s)
Left Saccade ← Coh → Right Saccade

Figure S5

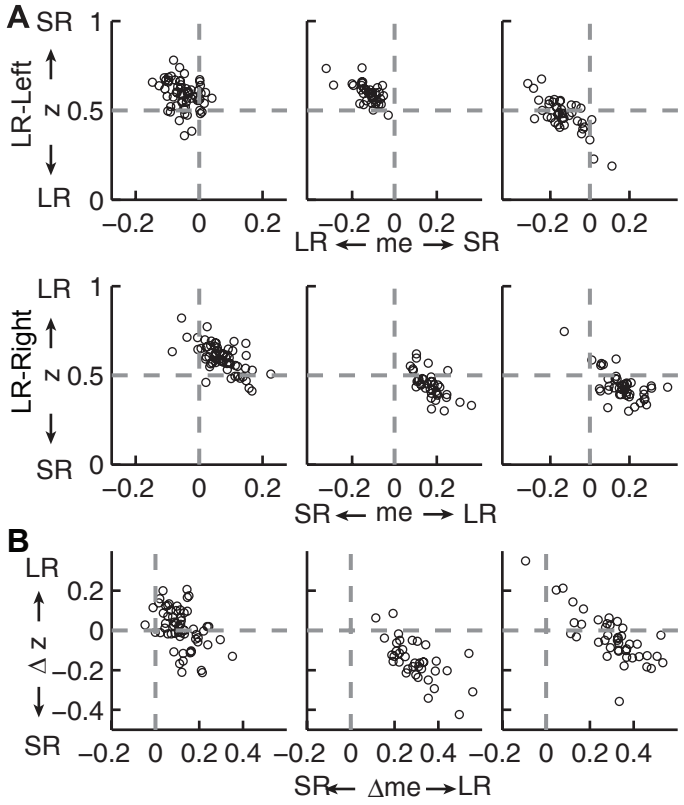
A
SR
LR-Left
z
LR
1
0.5
0
−0.2
0
0.2
LR ← me → SR
LR
LR-Right
z
SR
SR ← me → LR
B
LR
Δ z
SR
0.2
0
−0.2
−0.4
0.4
SR ← Δme → LR

Figure S6

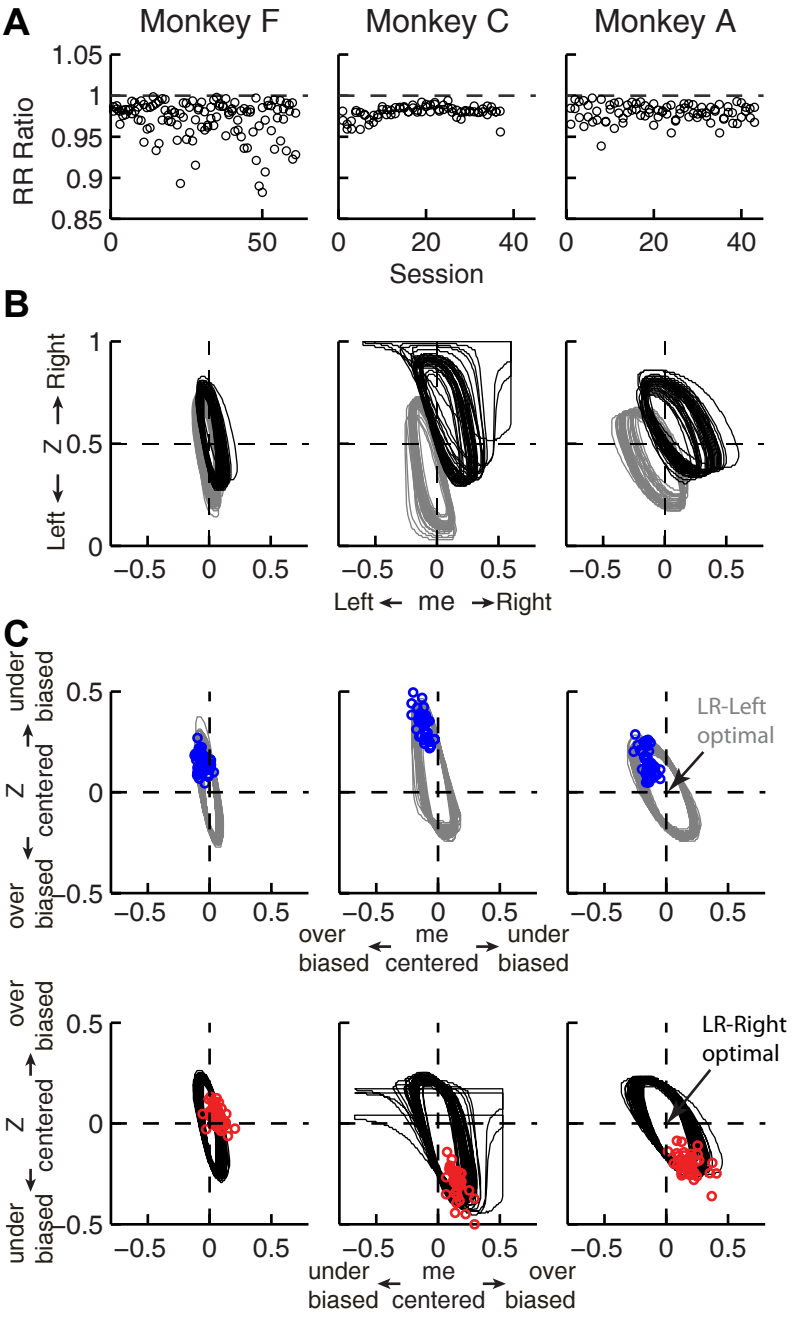
A
Monkey F
Monkey C
Monkey A
RR Ratio
1.05
1
0.95
0.9
0.85
0
50
0
20
40
0
20
40
Session
B
Left ← Z → Right
1
0.5
0
−0.5
0
0.5
Left ← me → Right
C
under biased
Z
over biased
centered
0.5
0
−0.5
LR-Left optimal
over biased ← me → under biased
centered
LR-Right optimal
under biased ← me → over biased

Figure S7

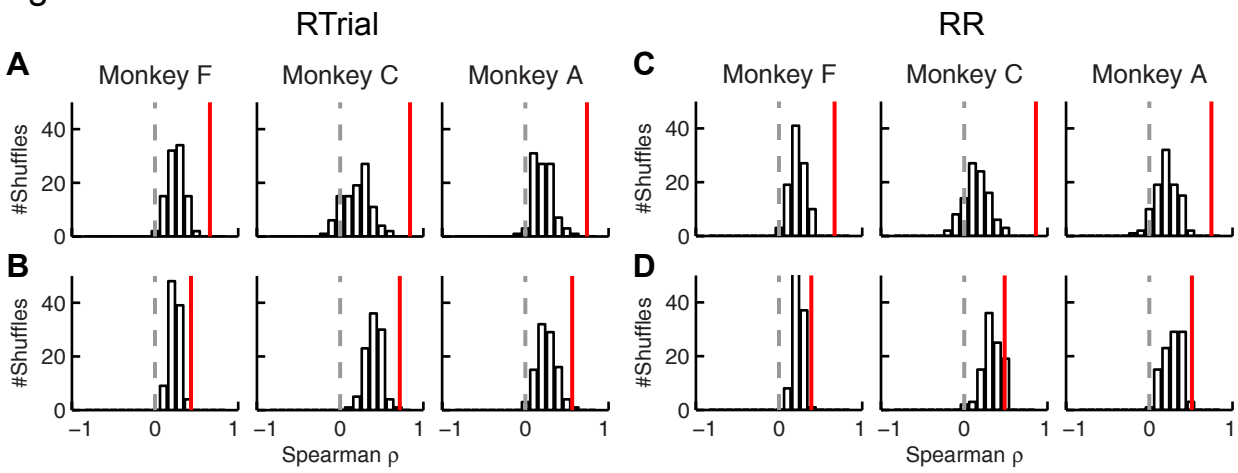
RTrial
RR
A
B
C
D
Monkey F
Monkey C
Monkey A
#Shuffles
0
20
40
−1
0
1
Spearman ρ

Figure S8

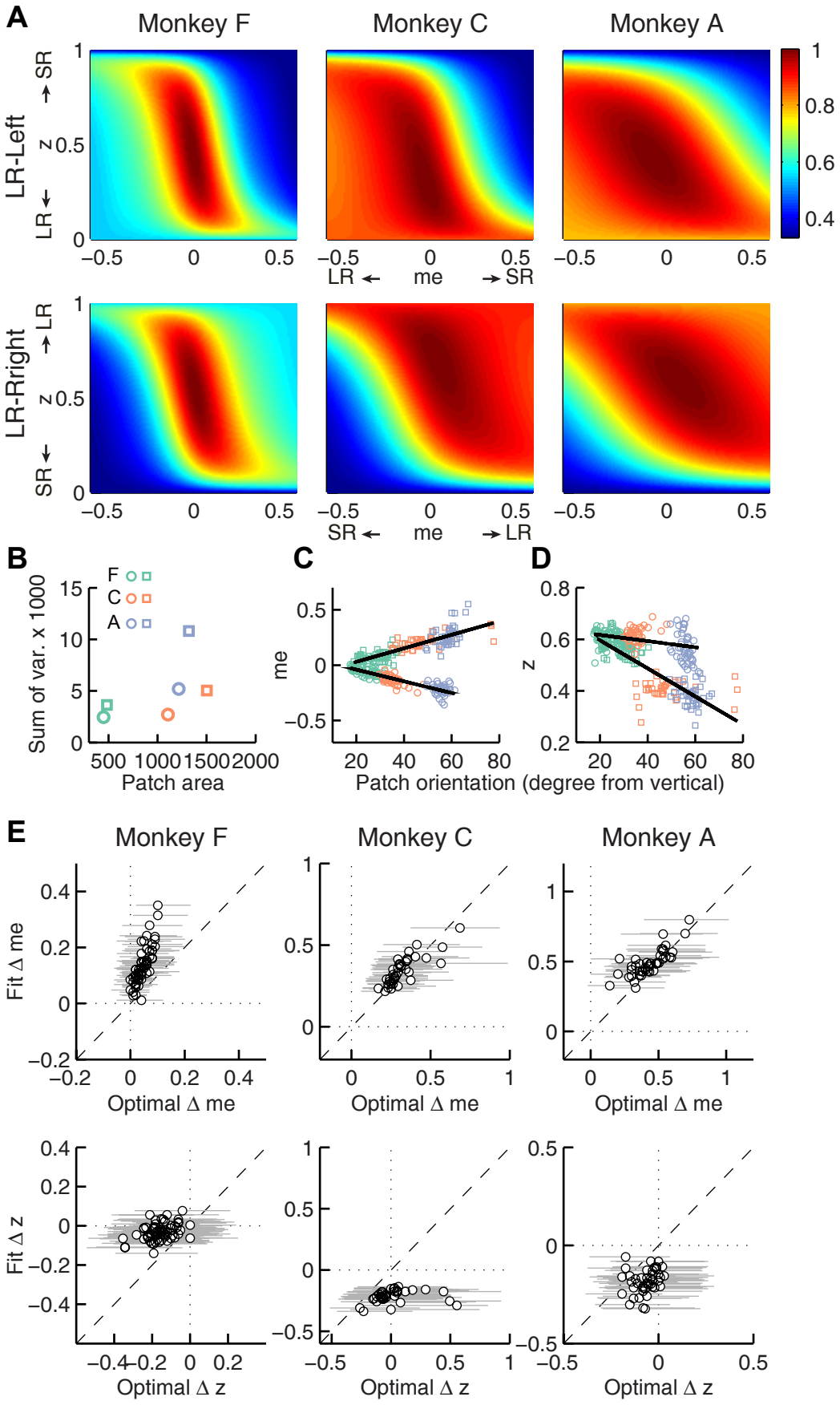
A
Monkey F
Monkey C
Monkey A
LR-Left
LR ← z → SR
LR-Rright
SR ← z → LR
LR ← me → SR
SR ← me → LR
B
Sum of var. x 1000
Patch area
C
me
D
z
Patch orientation (degree from vertical)
E
Fit Δ me
Optimal Δ me
Fit Δ z
Optimal Δ z

Figure S9

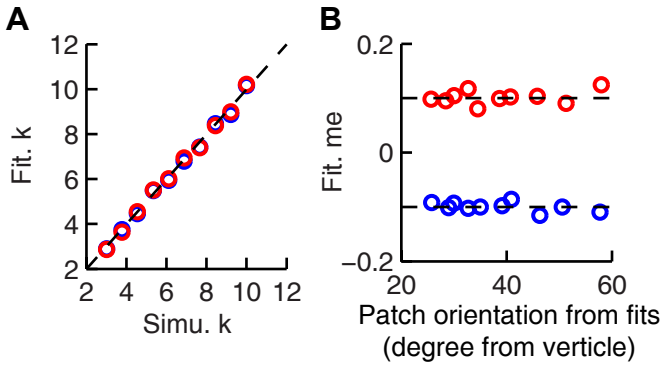
A
12
10
8
6
4
2
Fit. k
2 4 6 8 10 12
Simu. k
B
0.2
0
−0.2
Fit. me
20 40 60
Patch orientation from fits
(degree from verticle)

Figure S10

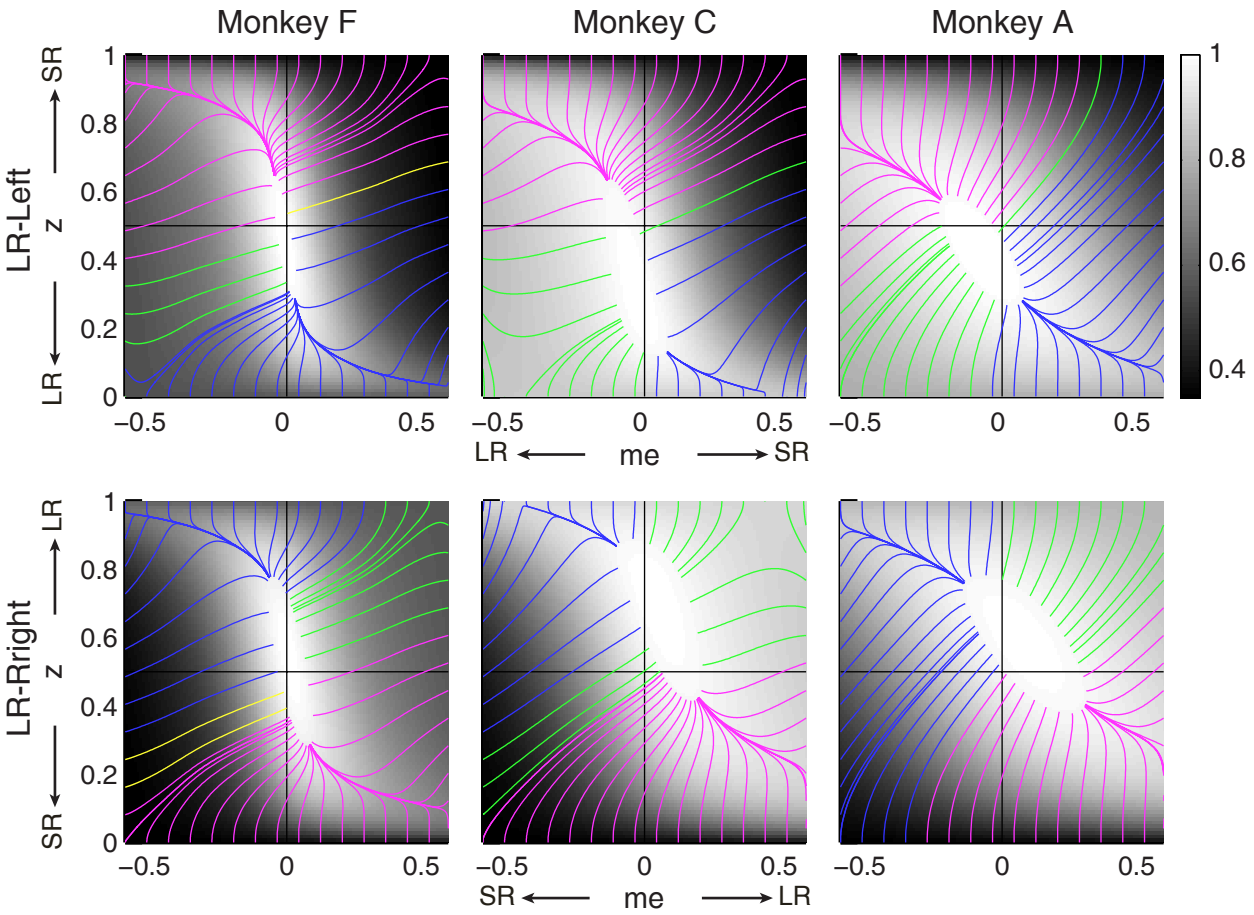

Trajectory end-point	me	z
	Over biased	Under biased
	Under biased	Over biased
	Over biased	Over biased
	Under biased	Under biased

Figure S11

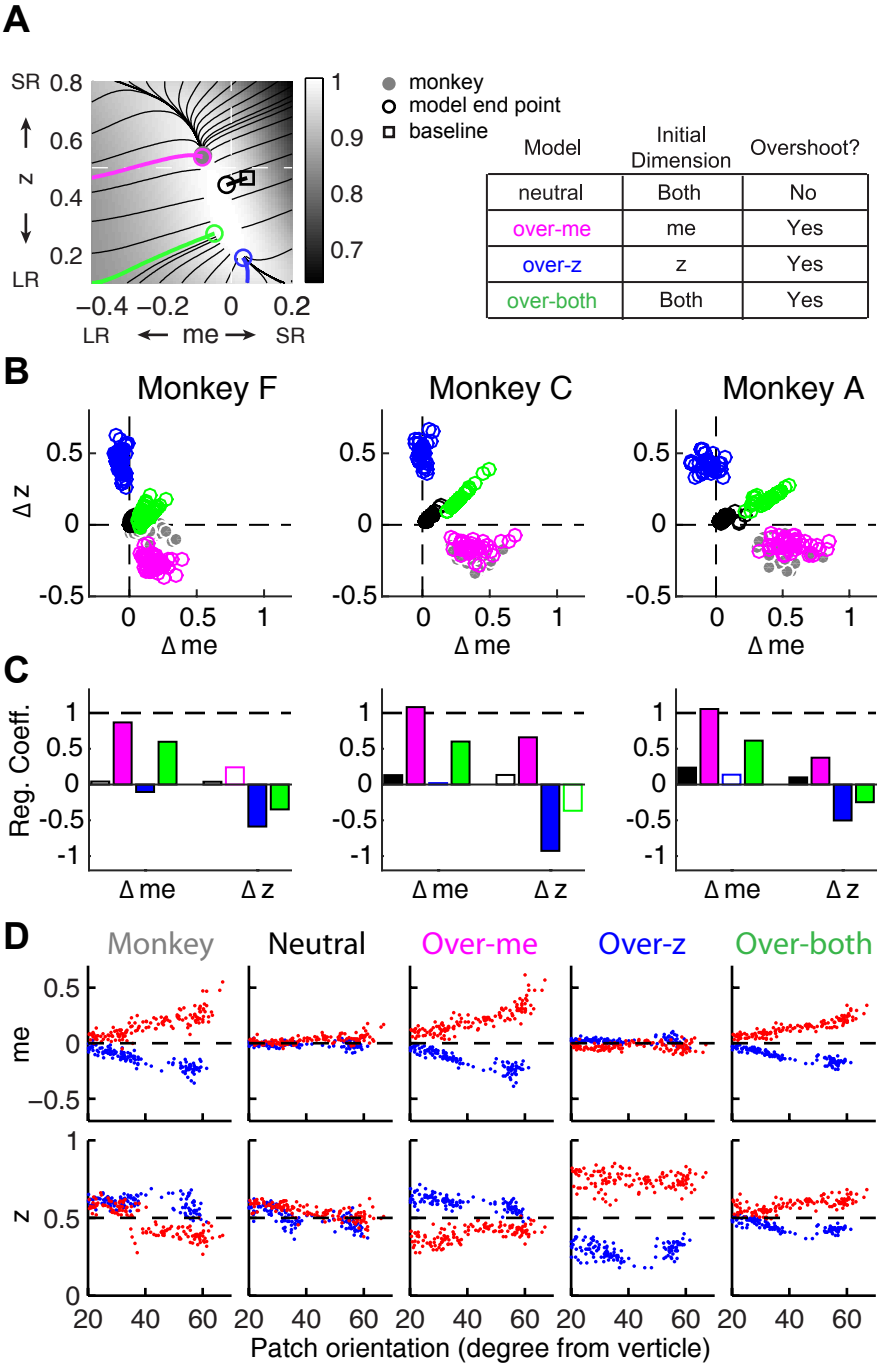

Model	Initial Dimension	Overshoot?
neutral	Both	No
over-me	me	Yes
over-z	z	Yes
over-both	Both	Yes

Figure S12

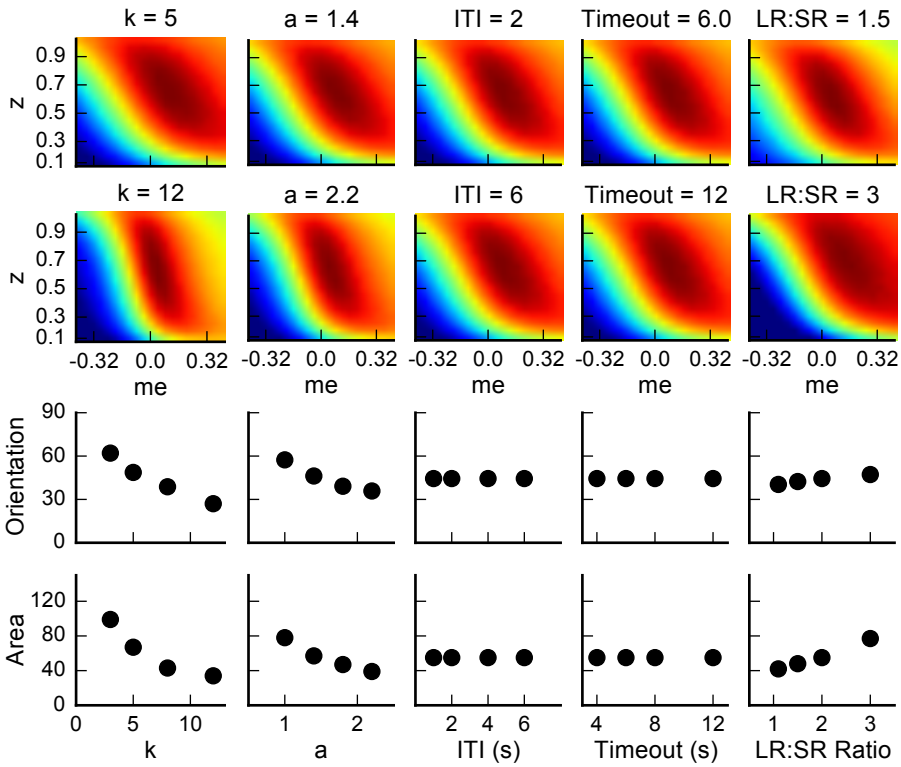
k = 5
a = 1.4
ITI = 2
Timeout = 6.0
LR:SR = 1.5
k = 12
a = 2.2
ITI = 6
Timeout = 12
LR:SR = 3
z
0.9
0.7
0.5
0.3
0.1
-0.32
0.0
0.32
me
Orientation
90
60
30
0
Area
120
80
40
0
5
10
k
1
2
a
2
4
6
ITI (s)
4
8
12
Timeout (s)
1
2
3
LR:SR Ratio